Published in final edited form as:

Glia. 2023 October ; 71(10): 2473–2494. doi:10.1002/glia.24436.

Microglial Nogo delays recovery following traumatic brain injury in mice

Elliot J. Glotfelty[1,2], **Shih-Chang Hsueh**[1], **Quia Claybourne**[3], **Alicia Bedolla**[4], **Katherine O. Kopp**[1], **Tonya Wallace**[5], **Binhai Zheng**[6], **Yu Luo**[4], **Tobias E. Karlsson**[2], **Ross A. McDevitt**[3], **Lars Olson**[2], **Nigel H. Greig**[1]

[1]Drug Design & Development Section, Translational Gerontology Branch, Intramural Research Program National Institute on Aging, NIH, Baltimore, MD 21224, USA

[2]Department of Neuroscience, Karolinska Institutet, Stockholm, Sweden

[3]Comparative Medicine Section, National Institute on Aging, NIH, Baltimore, Maryland 21224, USA

[4]Department of Molecular Genetics and Biochemistry, College of Medicine, University of Cincinnati, Cincinnati, OH, USA

[5]Flow Cytometry Unit, National Institute on Aging, Baltimore, MD, USA

[6]Department of Neurosciences, School of Medicine, University of California San Diego, La Jolla, CA, USA

Abstract

Nogo-A, B, and C are well described members of the reticulon family of proteins, most well known for their negative regulatory effects on central nervous system (CNS) neurite outgrowth and repair following injury. Recent research indicates a relationship between Nogo-proteins and inflammation. Microglia, the brain's immune cells and inflammation-competent compartment, express Nogo protein, although specific roles of the Nogo in these cells is understudied. To examine inflammation-related effects of Nogo, we generated a **mi**croglial-specific inducible **No**go **KO** (MinoKO) mouse and challenged the mouse with a controlled cortical impact (CCI) traumatic brain injury (TBI). Histological analysis shows no difference in brain lesion sizes between MinoKO-CCI and CControl-CCI mice, although MinoKO-CCI mice do not exhibit the levels of ipsilateral lateral ventricle enlargement as injury matched controls. Microglial Nogo-KO results in decreased lateral ventricle enlargement, microglial and astrocyte immunoreactivity, and increased microglial morphological complexity compared to injury matched controls, suggesting decreased tissue inflammation. Behaviorally, healthy MinoKO mice do not differ from control mice, but automated tracking of movement around the home cage and stereotypic behavior such as grooming etc. (termed cage "activation") following CCI is significantly elevated. Asymmetrical motor function, a deficit typical of unilaterally brain lesioned rodents, was not detected in CCI

Corresponding authors: Elliot J. Glotfelty (Elliot.glotfelty@nih.gov); Lars Olson (lars.olson@ki.se); Nigel H. Greig (Greign@grc.nia.nih.gov).

Conflict of Interest

None

injured MinoKO mice, while the phenomenon was present in CCI injured controls one week post-injury. Overall, our studies show microglial Nogo as a negative regulator of recovery following brain injury. To date, this is the first evaluation of the roles microglial specific Nogo in a rodent injury model.

Graphical Abstract

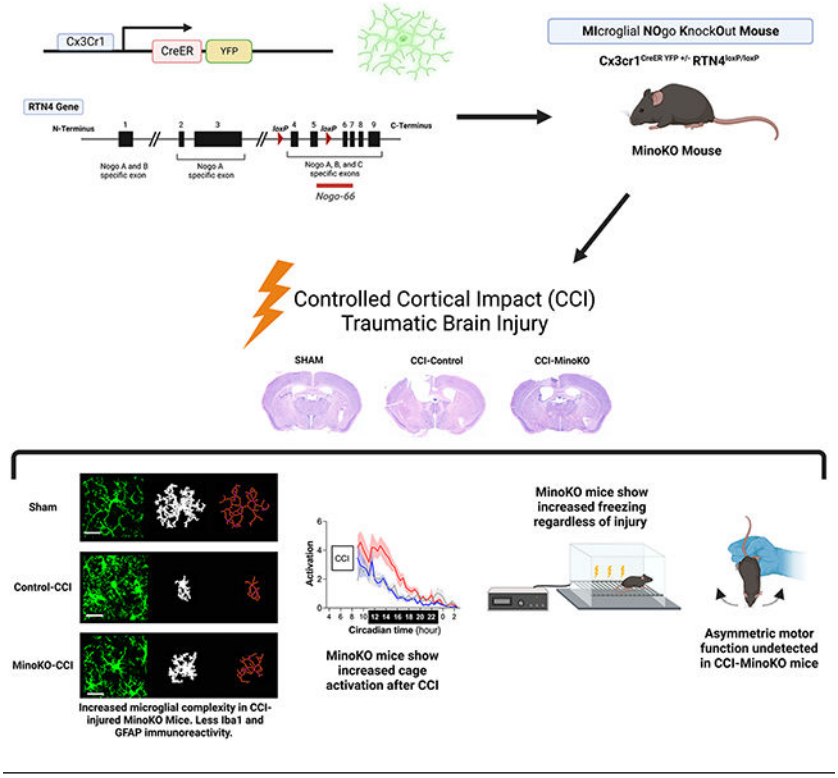

Introduction

The Nogo-signaling system, which encompasses a broad range of ligands, receptors and coreceptors, is known to delay or prevent critical repair systems following/during injury or disease. Signaling ligands, including Nogo-A, Nogo-B, and Nogo-C (Nogo proteins) all inhibit nerve growth activity via the Nogo-66 structural domain to the Nogo-66 receptor (NgR1), while Nogo-A signals through an additional domain known as amino-Nogo (Δ-20) (Schwab, 2010). Regardless of domain-receptor linkage, signaling is initiated, activating the GTPase ras homolog gene family member A (RhoA) and further downstream targets Rho-associated coiled-coil containing protein kinases (ROCK). This signaling program is involved in diverse and cell type-dependent signaling (Wikström et al., 2008; Xiang et al., 2013), but is most commonly known as a regulator of actin filament stabilization and growth cone stabilization.

Elevated levels of Nogo-A have been described in patients with a number of neuropsychiatric disorders, including temporal lobe epilepsy (Bandtlow et al., 2004), multiple sclerosis (Satoh et al., 2005), schizophrenia (Novak et al., 2002), and notably, Alzheimer's disease (AD) (Gil et al., 2006). In the AD patients, Nogo-A is elevated in

the hippocampus and localized to senile plaques around amyloid deposits that were also surrounded by reactive astrocytes. Interestingly, a reduction (deletion) of Nogo-A results in improved performance and neuropathology in AD transgenic (Tg) mice (Masliah et al., 2010). A recent study examining the cerebrospinal fluid (CSF) proteomes of AD (APP-PS1) and PD (A3P-αS) transgenic mice, showed reticulon 4 (RTN4, and also known as Nogo) was found at significantly higher levels in the aged-symptomatic mice but not in young asymptomatic control mice. Meta-analysis of astrocytic extracellular vesicles shows RTN4 as a prominent protein cargo, providing even further insight to how Nogo proteins may confer signaling (Heras-Romero et al., 2022).

Nogo protein distribution throughout subpopulations of cells within the brain may be a key factor in understanding the diverse roles that these receptors and ligands undertake in both chronic neurodegenerative disorders and acute injuries such as traumatic brain injury (TBI) or stroke. Focus on mouse models using single or combinatory global knockout (KO)/knockdown (KD) (Dickendesher et al., 2012; Zheng et al., 2005) or overexpression (Karlén et al., 2009; Karlsson et al., 2016) of Nogo receptors and KO/KD of Nogo proteins (Kim et al., 2003; Lee et al., 2010; Simonen et al., 2003; Yang et al., 2010; Zheng et al., 2003) provides important context to overall expression contributions to repair restricting properties of these proteins. In the context of injury repair, results have been mixed with genetic manipulations of these proteins especially on the regeneration of injured axons; however, there is consensus that Nogo and related proteins regulate the sprouting of uninjured axons (Zheng and Tuszynski, 2023) Germline KO of Nogo-related genes leaves open possible contributions of compensatory gene expression as animals develop, as previously shown (Simonen et al., 2003), making conditional KO studies possibly better suited to understand roles of these proteins in injury or disease models.

Antibody or peptide treatments targeting Nogo proteins are efficacious and contribute to repair following nervous system injury (Gonzenbach and Schwab, 2008; Thallmair et al., 1998; Zemmar et al., 2014; Zörner and Schwab, 2010) with timing of these treatments critical, especially in regards to stroke (Tsai et al., 2011). Efficacy results from targeting Nogo-related proteins in injury or disease models are more nuanced when examining specific cell type contributions. Indeed, cell type specific knockout of Nogo proteins are relevant, with preliminary studies of Nogo-A KO models in neurons (Vajda et al., 2015; Zemmar et al., 2017) and oligodendrocytes (Meves et al., 2018; Vajda et al., 2015; Zemmar et al., 2014) having differential affects in injury and disease models. With these models established, there is increasing interest for studies investigating the function of Nogo proteins in microglia, the immune cells of the brain, which are active during inflammatory diseases and injury states (Zhang et al., 2022). Antibodies against Nogo-A reduce protein expression of the canonical inflammatory cytokine tumor necrosis factor-alpha (TNF-α) in a retinal injury model (Baya Mdzomba et al., 2020). Silencing Nogo-A *in vitro* in PC12 cells via short hairpin (sh)-RNA interference resulted in decreased extracellular TNF-α and IL-6 in response to a lipopolysaccharide (LPS) challenge(Zhong et al., 2015). Additionally, Nogo was recently shown to play a key role in regulating pro-inflammatory gene production in macrophages (Arif Ullah et al., 2021). The Nogo-66 initiated signaling has been directly implicated in the production of inflammatory cytokines (Fang et al., 2015) with the

downstream RhoA-ROCK signaling cascade having clear involvement in the production of inflammatory cytokines (Glotfelty et al., 2023).

With the above in mind, we generated for the first time a microglial-specific inducible Nogo-A, B, and C KO mouse to investigate the role of microglial Nogo proteins in healthy and brain injured adult mice. As microglia are the resident immune cells of the brain and sources of neuroinflammation, our studies build upon the previous findings showing an inflammatory role of Nogo in a variety of *in vitro* and *in vivo* models. We employ a model of controlled cortical impact (CCI) of TBI, which we have previously used extensively in preclinical drug screening applications (Greig et al., 2019; Hsueh et al., 2022, 2021, 2019). Importantly, this model recapitulates many pathophysiological features apparent in moderate to severe human TBI (Glotfelty et al., 2019), which is one of the most prevalent causes of mortality among young children and the elderly worldwide. Animals were generated and subjected to a battery of behavioral testing prior to and after injury, with histological brain assessments performed two weeks after injury. We find that microglial Nogo deletion facilitates recovery following CCI injury as evidenced by these behavioral and histological assessments.

Methods

Animals

All procedures used in this study were fully approved by the Institutional Animal Care and Use Committee of the Intramural Research Program, National Institute on Aging, NIH (protocols #491-TGB-2023, #488-TGB-2022, and #331-TGB-2024). Studies followed the NIH guidelines for research on mice (DHEW publication 85–23, revised, 1995) and the current European Union regulations (Directive 2010 / 63 / EU) agreement number A1301310. To target genetic manipulation of microglial cells Cx3cr1$^{CreER\text{-}YFP/+}$ mice were obtained from Jackson Labs (Stock# 021160) and bred with Rtn4$^{loxP/loxP}$ mice (Meves et al., 2018) created by Binhai Zheng's group (available at Jackson Labs as Stock# 033364). The Cx3cr1$^{CreER\text{-}YFP+/-}$ have inducible Cre recombinase (CreER) and EYFP knocked into the Cx3cr1 locus, a gene specific to microglial cells of the brain and peripheral macrophages. The RTN4$^{loxP/loxP}$ mice have loxP sites inserted to flank the first and second common exons of the three isoforms of Nogo: Nogo-A, Nogo-B, and Nogo-C (Meves et al., 2018). Through multiple stages of breeding, we generated a conditional and inducible **Mi**croglial **No**go **K**nock-**O**ut (MinoKO) mouse with confirmed genotypes heterozygous for CreER-YFP and homozygous for the floxed RTN4 gene: Cx3Cr1$^{CreEr\ YFP\ +/-}$RTN4$^{loxP/loxP}$. One potential concern for the development of the MinoKO mouse is an effect from the heterozygosity of the Cx3Cr1 gene, as the Cx3cr1^{creER} mouse utilizes a knockout/knockin strategy for insertion of the CreER, and several studies have shown different phenotypes from Cx3Cr1 loss, though most severe in complete KO of the gene (Cardona et al., 2015; Rogers et al., 2011; Wang et al., 2021). For this reason, we incorporate two control animals for comparison to the MinoKO mouse to ensure any effects observed can appropriately be attributed to loss of microglial Nogo. Control animals for the studies include the 1) Cx3cr1$^{CreER\text{-}YFP+/-}$ mice heterozygous for the CreER-YFP insertion and exhibiting wildtype RTN4 expression (Cre Control) and 2) the original RTN4$^{loxP/loxP}$ animals (Floxed

control) which retain wildtype Cx3Cr1 expression (Fig. 1A). All genotyping was performed by contract through TransnetYX using a real time (RT)PCR assay with genetic material obtained from minimally invasive ear punches. For experimental use, MinoKO and Cre control mice were injected with tamoxifen (TAM) to activate Cre, and in MinoKO mice, remove the RTN4 gene via recombination. Floxed control mice were injected with vehicle (corn oil + 10% EtOH). The Cx3Cr1 promoter is one of the most widely used to specifically target microglial specific Cre expression, and importantly, with Cre not driving any adverse phenotypes or activation of microglia in adult mice (Vorhees and Williams, 2006). Although widely used for microglia studies, this promoter also targets peripheral macrophages, which have a much faster turnover rate than microglia. All animals in the current study were mature adults (ages 3-6 months) at time of experimentation, barring two older MinoKO females (8.6 months) that were used as sham animals in CCI experiments. Animals were kept on a normal 12h day-night cycle and were allowed access *ad libitum* to water and mouse chow. All behavioral testing was conducted during the light phase (day) cycle.

Tamoxifen Treatment

TAM (Sigma, cat# T5648) was first suspended in pure EtOH (Sigma, cat# E7023) with brief vortexing followed by addition of sterile corn oil (EtOH final concentration 10%). The TAM solution was then placed in a sonication bath for two minutes, with repeated sonication until fully dissolved. Final concentration of TAM was 20 mg/mL. MinoKO and Cre control animals were treated with alternating intraperitoneal (i.p.) injections for 5 consecutive days with a dosage of 100 mg/kg, each day; floxed control animals received vehicle injections relative to their weight. TAM administration in *Cx3cr1-CreER* mice produces active Cre and recombination in circulating monocytes/macrophages in the periphery. Thus, we waited approximately six weeks before inducing injury so recombined circulating monocytes turnover to non-recombined monocytes (Yona et al., 2013) so that resident microglia of the brain, which have much slower turnover rates, were the majority of cells with RTN4 deletion (Figure 1B) upon any experimentation.

FACS isolation of microglia

Methods used for isolating microglia are described in Hammond et al. (2019) with modifications. While anesthetized (under isofluorane), mice were subjected to a transcardial perfusion using 20 mL of ice-cold Hank's balanced salt solution (HBSS) without magnesium or calcium. Steady flow of HBSS was controlled via a 20 mL plunger syringe. Brains were carefully extracted from each mouse for separate processing. Each brain was individually minced into small pieces using a scalpel, followed by Dounce homogenization in a 15mL volume of HBSS on ice. Cell suspensions were individually filtered through a pre-wet 100 mm filter into a 50 mL conical tube with an additional 5 mL used to rinse the filter of any residual suspension. The tubes were centrifuged at 500 × g for 7 mins at 4°C. Following supernatant removal, cell pellets were loosened and suspended in 2 mL of 37% isotonic Percoll (GE Healthcare) and centrifuged for 30 minutes at 600 × g at 4°C. Cell debris and Percoll solution were aspirated off the cell pellet. The remaining Percoll was washed from the cell pellet using 1 mL of ice cold HBSS and centrifugation of 5000 × g for 30 seconds.

Cells were resuspended in 100 μL FACS staining buffer (HBSS without calcium or magnesium, 1mM EDTA, and 0.5% UltraPure BSA) and incubated in TruStain FcX™ Block (BioLegend) for 10 minutes followed by subsequent addition of P2Ry12- BV605 (SA011F11, BioLegend), CD11b- 488 (M1/70, Invitrogen, cat#53-0112-80), and CD45-APC (30-F11, Invitrogen) antibodies at manufacturer recommended dilutions (1 μg/ 100μL, 0.125μg /100 μL, 0.5 μg/100 μL, and 0.125 μg/100 μL, respectively) for 30 minσ on ice. Unbound antibodies were washed by addition of 1 μL of FACS staining buffer and a 30 sec centrifugation at 5,000×g. Cells were resuspended in 0.5 mL of FACS staining buffer and placed on ice. Cells were sorted using a Beckman Coulter Moflo XDP with a 70 μm nozzle, sheath pressure of 39psi, and a sample flow rate of 2000-3000 cells/second. Samples were collected on ice cold 100 μL FACS collection buffer (HBSS, 1mM EDTA, and 1% UltraPure BSA) in RNAse free 500 μL tubes. Live cells were gated from isolated cell populations, followed by a doublet exclusion step and subsequent gating via antibody stains. Control samples for P2Ry12 and Cd11b alone and unstained cells were used to establish the gating strategy for cells of interest (Fig. 1D).

qRT-PCR

Immediately following FACS sorting, RNA was isolated from microglia using the Applied Biosystems Arcturus™ PicoPure™ Isolation kit (cat# KIT0204) according to the recommended protocol (final elution volume of 15 μL). RNA quality and concentration was assessed via the Agilent 2100 Bioanalyzer using the RNA 6000 Pico Kit (cat # 5061-1513). RNA samples with RNA integrity number of 7+ were used for downstream qRT-PCR. Using RNA samples, cDNA was synthesized using random primers and RNase H+ MMLV reverse transcriptase via Bio Rad iScript reverse transcription supermix reagent and protocol (Bio Rad, 1708841).

To confirm efficient recombination/excision of the target region, PCR primers were selected to target a region within the floxed sites. Relative expression of genes was quantified using the delta Ct method compared to HPRT1 as a reference gene. Primers and carboxyfluorescein (FAM) labeled probes (or premixed set) used in the quantitative RT-PCR are listed in Table 2.

Controlled Cortical Impact (CCI) Traumatic Brain Injury

TBI studies were conducted in mature adult male and female mouse (25–35 grams, ages 3-6 months, with two older mice) (Table 1). Mice were assessed using a variety of behavioral tests before and after CCI injury, which are outlined below. Subsequently, brains were collected and evaluated for gross anatomical changes using histology and immunohistochemistry after euthanasia.

For CCI and sham procedures, mice were anesthetized with 2.5% tribromoethanol (Avertin: 250 mg/kg; Sigma, St. Louis, MO, USA), placed in a mouse stereotaxic frame (Kopf Instruments, Tujunga, CA, USA), and fixed with ear bars and an incisor bar. Skin was retracted under sterile conditions and a 5-mm square craniectomy was performed over the right motor cortex at the posterior corner between the bregma and sagittal sutures. Using a drill, the skull was carefully removed, avoiding damage to the dura or to the temporalis

muscle. The CCI device, Impact One (Leica Biosystems Inc., Buffalo Grove, IL, USA), consists of an adjustable electromagnetic impactor with independent contact velocity and the depth control for cortical deformation. Prior to impact, the tip of the 3-mm flat impactor was adjusted to be perpendicular to the exposed cortical surface. The contact velocity was set at 5 m/s, dwell time at 0.2 s, and a deformation depth of 1 mm in order to produce a moderate TBI. Following the CCI procedure, sterile cotton-tipped applicators were used to clean the area around the injury site, which was quickly then closed with surgical sutures (Ethicon Inc., Somerville, NJ, USA). Sham animals were anesthetized and followed the same procedure as TBI mice without CCI impact. During surgery and recovery, the core body temperature of all mice was maintained at 36–37 °C using a heating pad and heated chamber, respectively. Mice were returned to their home cage after awakening from anesthesia, and for pain relief, were administered a 72-h sustained release buprenorphine solution (SR-LAB) (ZooPharm) at a dose of 1 mg/kg.

Histological Analysis

Mice were anesthetized with 5% isoflurane and perfused transcardially with ice cold 0.9% saline for blood clearing followed by and 4% paraformaldehyde (PFA) in 0.1 M phosphate buffer (PB, pH 7.2) for initial tissue fixation. Brains were removed and post-fixed for 24 hours in 4% PFA followed by sequential sucrose saturation (20% followed by 30% sucrose) in 0.1 M PB until the brain sank in each solution. Each brain was mounted and frozen onto a cryostat chuck using optimal cutting temperature (OCT) compound (VWR cat#361603E) chilled with dry ice. Brains were cut into 20 μm sections using a cryostat (Leica Biosystems Inc., Buffalo Grove, IL, USA). All slices were collected spanning the striatum to the hippocampus, with every seventh section selected for ventricle and injury/lesion size assessment. Sections were stored in −20°C cryoprotectant (30% glycerol, 30% ethylene glycol, 40% 1x PBS). Prior to mounting or staining slices, cryoprotectant was washed with 1 x PBS.

Giemsa Staining—Quantification of brain lesion and lateral ventricle size in TBI animals: Sets of selected serial brain slices from 2-week post-TBI or sham (20 μm) were mounted on slides and air dried. In a chemical fume hood, the sections were rehydrated in 1/15 M KH_2PO_4 (9.07 g/ L; Sigma, cat# P0662) buffer for 10 min followed by 30 min saturation in 10% Giemsa (Sigma, cat #12-0440) KH_2PO_4 buffered solution (pH 4.5) at 40 °C. afterward a brief rinse in KH_2PO_4 solution, the slides were de-stained and dehydrated in absolute ethanol (1 minute × 3). Sections were then cleared using a brief xylene (Sigma, cat# 534056) rinse and cover-slipped (Epredia™ Cytoseal™ 60, FisherScientific, cat#23-244257). Slides were scanned in an All-in-One Fluorescence Microscope BZ-X710 (Keyence Corporation of America, Itasca, IL, USA), and brain image areas were quantified using ImageJ 1.52q software (National Institutes of Health, Bethesda, MD, USA). The formula for injury ratio and lateral ventricle size was as follows: Σ area of ipsilateral hemisphere/ Σ area of contralateral hemisphere × 100; Σ area of ipsilateral lateral ventricle/Σ area of contralateral lateral ventricle × 100. There were 9 brain sections from each mouse counted, with regions starting from bregma 0.86 mm to −2.5 mm, spanning the injury site.

Brain slice immunohistochemistry—Free floating brain sections were washed with PBS to remove cryoprotectant and then permeabilized/blocked in tissue staining buffer (TSB) [1x PBS with 0.1% Triton-X 100 (SIGMA, Cat # T9284-500ML) and 3% bovine serum albumin (BSA) (Sigma, cat# A7030PBS) in PBS] for 1 h. A series of primary antibodies was prepared in the TSB, and the sections were incubated in this solution overnight at 4° C. Primary antibodies used include the following: anti-Iba1 (Ionized calcium binding adaptor molecule 1) (Synaptic Systems, cat # 234308, RRID:AB_2924932, dilution 1:500, raised in guinea pig), anti-GFP/YFP (Abcam, cat# ab290, RRID:AB_303395, dilution 1:500, raised in rabbit), anti-GFAP (Glial Fibrillary Acidic Protein) (Invitrogen, cat# PA1-10004, dilution 1:1000, raised in chicken), and anti-Nogo (SantaCruz, cat# 271878, dilution 1:50, raised in mouse). After incubation with primary antibody, the sections were washed three times for 5 mins with tissue wash buffer (TWB) (0.1% Triton-X 100 in PBS). Slices were then incubated for 2 h at room temperature in diluted (1:500 in TSB) Alexa-Fluor™ secondary antibodies (Thermo Fisher Scientific, Invitrogen) that corresponded to the targeted species of the paired primary antibody: goat anti-guinea pig-555 IgG (H+L) (cat# A21435, RRID:AB_2535856), donkey anti-mouse IgG (H+L) Highly Cross-Adsorbed-647 (cat# A32787, RRID:AB_2762830), donkey anti-rabbit IgG (H+L) Highly Cross-Adsorbed-488 (Cat# A-21206, RRID:AB_2535792), goat anti-guinea pig IgG (H+L) Highly Cross-Adsorbed-488 (cat# A-11073, RRID:AB_2534117), and goat anti-chicken IgY (H+L) Highly Cross-Adsorbed-647 (cat# A-21449, RRID:AB_2535866). Secondary only controls were used throughout experiments to ensure antibody specificity. The sections were then washed with TWB three times for 5 mins followed by a 5 min wash in 1x PBS. Slices were mounted on slides, secured with Antifade Mounting Medium with DAPI (Vector Laboratories, cat# H120010) and cover slipped. Endogenous YFP expression was not evident in fixed tissue without use of the GFP antibody, hence Iba1 images using the 488 fluorophore do not experience enhanced signal. Users imaging and evaluating images were blinded to genotypes and treatment groups.

Brain Slice Imaging—Four 20x images/fields of view z-stacks (20μm) were taken in brain regions of interest, the cortex and thalamus, on both the ipsilateral and contralateral sides of the brain, total of 16 Images/FOV per brain, using a Confocal Laser Scanning Microscope (Zeiss LSM880, Oberkochen, Germany) at the epicenter of the cortical injury. ImageJ2 (version 2.9.0/1.53t) (National Institutes of Health, Bethesda, MD, USA) (Rueden et al., 2017). Default thresholds were set for Iba1 and GFAP immunoreactivity from each 16-bit maximum intensity projection image with total area covered per binary image averaged across each animal, from images of each region.

Microglia morphology assessment—The four images/FOV captured from both the ipsilateral and contralateral hemispheres (cortex and thalamus) were used for microglial morphology assessments. Morphometric parameters of microglia (5-6 microglia/field of view) were analyzed using MotiQ, fully automated analysis software. MotiQ was developed as an ImageJ plugin in Java and is publicly available (https://github.com/hansenjn/MotiQ). The microglial ramification index (RI) is a unit free metric determined by calculation of the ratio of the cell surface area to the surface area of a perfect sphere with the same volume as the analyzed cell. An RI of 1 corresponds to a perfectly round cell without processes

while increasing cell processes are seen in more complex branching cells. Segmentation and quantification were performed on the maximum intensity projections of 16-bit TIFF images. Spanned area per cell, number of branch end points, and total length of tree skeleton were also assessed using MotiQ. Data represented here are averages of all microglia measured from each brain region.

Behavioral Assessments

A battery of tests were selected that would span domains of locomotor activity, emotion, and cognition. Behavioral tests with demonstrated confounding by repeated testing were only performed once, either before (Morris water maze (Vorhees and Williams, 2006) , elevated plus maze (File, 1993)) or after CCI (fear conditioning (Radulovic et al., 1998)). Other tests (home cage activity, open field, spontaneous alternation, asymmetrical body function) were performed both pre- and post-CCI.

Home cage activity tracking—Mice were singly housed with activity automatically tracked using the digital individually ventilated cage system (DVC™; Tecniplast). Animals were tracked for 42 days pre-CCI and 14 days post-CCI.

***Open Field Test* (OFT)—**Mouse activity levels were measured using the OFT. Mice were individually placed in a 44 x 44 x 30 cm clear Plexiglas arena, which was located inside a dimly lit sound-attenuating cubicle. Activity was monitored for 30 minutes using an array of infrared beams and tracking software (MED-Associates; St Albans, VT).

Elevated Plus Maze—Mice were placed for five minutes in an opaque beige elevated plus maze consisting of four arms radiating at 90 degree angles, sitting 38.7 cm above the floor. Arms were 5.1cm wide and 30.5cm long; two opposing arms were enclosed with 15.2cm high walls; the other two arms had a 3mm lip. Activity was recorded by an overhead camera and analyzed using ANY-Maze software (Stoelting Co; Wood Dale, IL).

Spontaneous Alteration Test—Mice freely explored for 15 minutes in an opaque red plexiglass maze containing four arms (5 wide, 30 cm long, 25 cm tall) radiating from the center at 90 degree angles. Arm entries were automatically detected using an overhead camera and ANY-Maze software. Alternations were scored as sequences of entries into three unique arms without repeats (e.g., ABCD or BCDA but not ABAC or ABBD). Alternation rate was calculated as number of alternations divided by number of opportunities (total arm entries – 3).

Morris Water Maze (MWM)—Prior to water maze training, mice were habituated with a 60-second exposure to 25°C water in a small tub (30 cm diameter) containing a 7cm diameter round submerged platform. Beginning the next day, mice were trained to locate a square platform submerged 1 cm below the surface of the water in a larger tub 140 cm in diameter. To facilitate climbing, the platform consisted of three 0.5 cm high steps that were 12.5 cm across at the bottom and 9.5cm across at the top. Water was made opaque by the addition of non-toxic white tempera paint and maintained at 22 ± 0.5°C for males and 24 ± 0.5°C for females. Mice were given 4 trials per day with a minimum inter-trial interval of

10 minutes. If mice did not find the platform in 60 seconds, they were gently guided to it. Mice remained on the platform for 20 seconds before being returned to their home cage. At 24 hours following the last day of training, a 60 second probe trial was conducted without platform to assess memory for platform location. To confirm motivation & ability to swim to a platform based on visual cues, a visible platform control test was run following probe testing. Prominent visual cues were added to the platform itself, and mice were given 4 trials to locate it.

Fear Conditioning—Fear conditioning was conducted over three days in a standard chamber with a side-mounted camera and automated computer scoring (MED-Associates; St Albans, VT). On training day mice were placed in the chamber for a two minute baseline, followed by a 30-second tone (10 kHz, 85 dB) that co-terminated with a two second, 0.5mA scrambled shock delivered by stainless steel floor bars. After a 60 second inter-stimulus interval (ISI), a second tone-shock pairing was delivered. Mice remained in the chamber for two minutes and were returned to home cage. Contextual conditioning was measured 24 hours later (recovery) as mice were placed into the chambers for five minutes. Cued conditioning was tested 24 hours after the context test in chambers that contained modified floor, ceiling, lighting, and odor to differentiate from the conditioning environment. After a two minute baseline period, the auditory cue was presented for three minutes.

Asymmetrical Motor Function—Body asymmetrical motor function was assessed using the elevated body swing test (EBST), as initially described by Borlongan et. al (1995). Briefly, animals were examined for lateral movement/turning when their bodies were suspended 10 cm above the testing table. The animals were lifted from the table while held by the base of the tail. A left/right swing was counted when the head/torso of the animal moved more than a 10° angle from its vertical axis after elevation. The frequency of the left/right swings was scored across 20 consecutive trials. An uninjured animal generally shows a tendency to equally swing to either side. Animals with unilateral brain lesions or damage, tend to swing towards the uninjured (contralateral side) as the uninjured hemisphere dominates function. The number of ipsilateral and contralateral swings was determined and used to create a percentage of contralateral swings, which then was statistically analyzed. Experimental users were blinded to genotype when performing this task.

Statistical Analyses

Statistical analyses were performed using R version 3.6.1 and GraphPad Prism. Tests with single data point were analyzed first using linear modeling with terms for treatment. Tests with repeated testing were analyzed using linear mixed effects modeling (R package nlme) with terms for treatment, sex, and time. "Treatment" was defined in pre-CCI tests as one of the three genotype groups (Floxed control, Cre Control, or MinoKO). In all post-CCI tests except fear conditioning there were no differences between genotypes after controlling for sex and CCI/sham treatment; therefore “Treatment” term in reported analysis grouped animals into Sham-Control (all genotypes), Control-CCI (two control genotypes combined), or MinoKO-CCI . Because genotype had a significant main effect in fear conditioning, the “Treatment” term was replaced with separate terms for “Genotype”, “CCI”, and their interaction. Post-hoc pairwise comparisons made with Tukey’s HSD. Significance cutoff

was p=0.05 in all tests. Pre- and post- behavioral/histological statistics, including effect of sex and sex × treatment are provided in Tables S1 and S2, respectively.

Results

Development of MinoKO mouse

We used three different genotypes of mice in the current experiments; two control lines, 1) which expressed CreER in microglia (Cre Control) and 2) another with no CreER but floxed RTN4 sites (Floxed Control), and 3) the MinoKO mouse which expresses CreER in microglia and also has a floxed RTN4 gene (Fig. 1A). Cx3Cr1 is a gene specific to microglia and circulating macrophages and its promoter is used to drive expression of CreER in these cells, driving efficient recombination of a floxed gene of interest (Bedolla et al., 2023). RTN4 gene translation results in production of three isoforms of the Nogo protein, Nogo-A, -B, and -C which we have targeted with floxed sites in a biologically active region of all three forms, the Nogo-66 site (Fig. 1B). CreER-YFP expression in MinoKO mice is highly specific for microglial cells, indicated by strong colocalization of immunochemical staining signal of YFP to ionized calcium binding adaptor molecule 1 (Iba1) (Fig. 1C). Microglia were isolated via FACS from Floxed Control, TAM treated Cre Control, and TAM treated MinoKO mice using microglial-specific antibodies anti-P2Ry12 and anti-Cd11b, with some contribution in signal from endogenous YFP expression (Fig. 1D). mRNA isolated from each sample was processed using RT-qPCR and assessed for levels of Exon-4 and Exon-5 of the RTN4 gene. We probed mRNA within the Floxed region of the gene. Two-way ANOVA revealed differences between groups ($F_{2,23}$=186.4, p<0.0001), with no significant differences in gene expression for Exon-4 (p=.6807) or Exon-5 (p=.7976) between Floxed and TAM treated Cre Control mice, and significant decreases in the TAM treated MinoKO mice for both exons compared to both controls (p<.0001) (Fig. 1E). This is indicative of effective recombination and alteration of Nogo expression in microglia.

Previous Nogo KO animal models have targeted different locations on the RTN4 gene, specifically the Nogo-A specific active region (Δ-20) (Dimou et al., 2006; Kim et al., 2003; Simonen et al., 2003), while this current study targets the Nogo-66 region common to all three Nogo protein isoforms. Simonen and colleagues (2003) show that deletion of only the Nogo-Aactive region resulted in increased protein expression of Nogo-B, highlighting a possible compensatory shift in Nogo protein when only the Δ-20 region is removed. Studies targeting a similar region of RTN4 as the current study resulted in null expression or a hypomorph of all three Nogo proteins (Zheng et al., 2003).

Microglial Nogo does not affect locomotion, anxiety, or spatial memory in healthy adult mice

We assessed if microglial Nogo KO has any effect on the behavior of healthy mice, including activity levels, spatial memory, and motor function (Fig. 2A). Home cage activity (Fig 2B) was monitored by capacitive sensors located underneath each cage (Pernold et al., 2019), with female mice showing overall more activity (Table S1) as has been previously described (Konhilas et al., 2015; Oydanich et al., 2019). light phase activation varying by sex ($F_{1,18}$=5.34,p=0.03) but not genotypes ($F_{2,18}$=2.23,p=0.14) (Fig. 2Ci). Results were

similar for dark phase activity, also differing by sex ($F_{1,18}$=9.74, p=0.006) but not group ($F_{2,18}$=0.21, p=0.8) (Fig. 2Cii). Distance traveled ($F_{2,18}$=0.92, p=0.4) (Fig. 2D) and time spent in the center square of an open field apparatus (not shown) did not differ between groups or by sex (Table S1). Accordingly, anxiety-like behavior in the elevated plus maze (EPM), assessed by time in the open arms, was not statistically different between groups ($F_{2,18}$=0.23, p=0.8) (Fig. 2E). Spatial working memory was assessed by measuring continuous spontaneous alternation (Hughes, 2007) in a 4-arm "cross maze" (Jawhar et al., 2012). Alternation rate did not differ between groups ($F_{2,18}$=1.02, p=0.4) (Fig. 2F). Spatial learning and memory was assessed using the Morris water maze (Morris, 1984). Escape latencies improved over time across all groups ($F_{3,54}$=16.56, p<0.0001) but did not differ between groups ($F_{2,18}$=0.23, p=0.8) (Fig. 2G). Retention during a 24-hour probe test, assessed by time searching in the quadrant that had previously contained the hidden platform(Fig. 2H), did not differ between groups ($F_{2,18}$=2.14, p=0.15).

Microglial Nogo deletion reduces lateral ventricle enlargement following CCI injury

Gross pathology associated with the CCI induced TBI was assessed following histological staining of a series of brain slices within the impact region (Fig. 3A). Injury size from CCI is shown as an average percentage of ipsilateral to contralateral hemisphere. CCI resulted in significant tissue loss compared to sham injured group ($F_{2,21}$= 6.536, p=.0062) in both the CCI controls (p=.0237), including both the Floxed and Cre Control animals, and MinoKO mice (p=.0084). CCI injured animals showed no differences when compared to each other (p=.8882) (Fig. 3B).

We further assessed the lateral ventricle size as a metric for changes in intracranial CSF following the TBI. This is a common pathological feature observed in human TBI patients (Levin et al., 1981). Ventricle size is shown as an average ratio between ipsilateral and contralateral ventricles across all brain sections assessed (Fig. 3C). Despite a slightly more significant injury size, MinoKO mice do not show differences in ipsilateral lateral ventricle size versus sham injured animals (Figs. 3C & 3D).

No sex differences were observed regarding the tissue loss or lateral ventricle enlargement (Table S2).

Microglial Nogo deletion decreases microglia and astrocyte reactivity following CCI injury

Microglia and astrocytes are sources of neuroinflammation and are prevalent drivers of pathology in human TBI and neurodegenerative disease (Glotfelty et al., 2019). Microglial activation is most dominant in the cortex near regions affected by the TBI impact, but damage to corticothalamic tracts also initiates prominent microglial activation patterns in the thalamus (Ramlackhansingh et al., 2011; Scott et al., 2015). Our group and others have previously demonstrated this using the CCI TBI model (Donat et al., 2016; Hsueh et al., 2022, 2021). Representative immunochemical staining of $Iba1^+$ microglia (Fig. 4A) is shown in both the cortex and thalamus, resulting in significant elevations of Iba1 coverage in the ipsilateral cortex and thalamus of both CCI injured Control and MinoKO mice compared to Sham animals (Fig. 4B, 4C) (p<.0001 and p<0.001, respectively), with no effect observed across groups on the contralateral side of the brain (Table S2). CCI injured MinoKO mice

show significant reductions in ipsilateral Iba1 coverage compared to CCI Controls in both the cortex ($p<.0001$) and thalamus ($p=.0166$) (Fig. 4B, 4C). Overall, female mice showed less Iba1 immunoreactivity in the cortex than males irrespective of group ($p=.002$) with no sex × treatment interaction. Crosstalk of microglia and astrocytes during injury and disease also leads to elevated levels of GFAP in astrocytes (Liddelow et al., 2017). Hence, we assessed GFAP immunoreactivity (Fig. 4A), which is significantly elevated in the ipsilateral cortex of both the CCI Control and MinoKO mice compared to Sham mice ($p<.0001$). CCI injured MinoKO mice show reductions in GFAP coverage in the ipsilateral cortex compared to CCI injured Control mice ($p=.012$) (Fig. 4D).

We further assessed individual morphologies of microglia in the cortex and thalamus using the *MotiQ* software in FIJI. Microglial morphology provides a gross representation of the activation state of individual cells. Microglia in a healthy brain maintain many processes to perform homeostatic functions. These microglia are traditionally described as “ramified” while injury or disease states can produce rounder “reactive” microglia with decreased process length and ramification. In even more highly inflammatory environments, such as sites of severe injury, “amoeboid” microglia with very few short or no processes are observed. Decreased ramification and process complexity is generally considered to be indicative of a more inflammatory environment, though the complexity and diversity of microglial function does not fully lend precise functional differences to associate with each morphology subtype (Paolicelli et al., 2022). Three representative $Iba1^+$ microglia are shown for contralateral cortex and thalamus (Fig. 5A,i) with thresholded (5A, ii) and skeletonized (5A,iii) images produced via *MotiQ* accompanying. Representative microglia from CCI Control and CCI MinoKO mice are similarly displayed (Fig. 5A). Twenty microglia across four fields of view from each brain region/mouse were individually analyzed and values averaged. The CCI injury significantly reduced ramification of cortical (Fig. 5B, i) and thalamic (Fig. 5C, i) ipsilateral microglia in both CCI Control and CCI MinoKO mice ($p<.0001$) without affecting contralateral microglia from the same regions. Similar reductions in cortical and thalamic ipsilateral microglia spanned area (ii) (cortex: $p=.0002$; thalamus: $p<.0001$), endpoints (iii) (cortex and thalamus: $p<.0001$), and total tree length (iv) (cortex: $p=.0001$; thalamus: $p<.0001$) were observed compared to Sham injured ipsilateral microglia. Ipsilateral microglia from CCI injured MinoKO mice show significant increases compared to CCI Control mice in both the cortex and thalamus across nearly all parameters shown: (i) ramification (cortex: $p=.0406$; thalamus: $p=.0027$), (ii) spanned area (cortex: $p=.0385$; thalamus: $p=.0081$), (iii) endpoints (cortex: $p=.0074$; thalamus: $p=.0998$), and (iv) total tree length (cortex: $p=.0415$; thalamus: $p=.0439$). We did detect a sex difference in ipsilateral cortex endpoints ($p=.02$), indicating female mice have a higher number of microglial endpoints. Female mice were also shown to have increased total tree length compared to other males in the same group ($p=0.02$) No differences were observed across all contralateral microglia analyzed (Table S2), focusing our comparisons on ipsilateral microglia. Grubbs’ test was applied to all data to identify outliers. For cortical Iba1 immunoreactivity measurements in Figure 4B, one data point in the ipsilateral MinoKO-CCI was removed. One data point was also removed in the sham thalamic ipsilateral spanned area from Figure 5Cii. Overall, in response to the CCI injury, microglial immunoreactivity is reduced (Fig. 4) and individual cell complexity increased (Fig. 5) from Nogo deletion

in microglia. As Control-CCI microglia show reduced morphological complexity compared to the MinoKO-CCI microglia, they are more reactive to the injury and thus represent a morphology more likely to produce higher levels of pro-inflammatory cytokines (Kloss et al., 2001; Madry et al., 2018).Our previous work with the CCI-model (Hsueh et al., 2022) and transgenic AD mouse model (Lecca et al., 2022) shows that anti-inflammatory drugs increase, respectively, ipsilateral and overall microglial complexity, further evidence for reduced inflammatory profile of MinoKO-CCI microglia.

Following CCI injury, microglial Nogo deletion increases home cage activity/overall locomotion and increases freezing in a fear conditioning paradigm

We assessed a variety of behavioral parameters following the CCI procedure (Fig. 6A). Mice were singly housed their activity continuously monitored (Fig. 6B) as was undertaken prior to the CCI injury. Home cage activity during light phase (Fig. 6Ci) varied by date ($F_{7,215}$=44.71, p<0.0001) with increased activity across all groups immediately following CCI or sham procedures. This spike in home cage activation on the day of CCI treatment carried through into the dark phase only for MinoKO mice (Fig. 6Cii; CCI x date interaction $F_{14,124}$=2.86, p=0.0009; Tukey HSD CCI-MinoKO vs Control-CCI p=0.009; vs Sham p=0.04). A more detailed temporal analysis of activity following CCI administration (Fig 6D) demonstrated that CCI-MinoKO increased home cage activity was most pronounced during the first half of the dark phase. Female mice were more active than males two days following the CCI procedure (p=0.008), similar to results observed prior to injury. Home cage activity during the first 12 hours after CCI/sham administration differed between groups ($F_{2,18}$=12.55, p=0.0004), with post-hoc comparisons revealing differences between MinoKO-CCI and both CControl-CCI (p<0.001) and sham (p<0.01) (Fig. 6E). CCI produced a delayed reduction in activity: twenty-four hours later (night +1), Control-CCI mice were less active than Shams (Fig. 6Cii; Tukey HSD p=0.03). This effect was partially blunted in MinoKO-CCI mice, which did not differ from Sham controls (p=0.8). A detailed look at full circadian activity during this period (Fig. 6F) revealed that Control-CCI mice showed normal initial activity in response to lights out, but then grew less active whereas Sham and MinoKO-CCI mice showed bursts of activity throughout the dark phase. To quantify this phenomenon, we calculated the average activity starting 2 hours after lights off through 2 hours after lights on at the end of night +1 (Fig. 6G). Here Control-CCI mice were significantly less active than Sham controls ($F_{2,17}$=5.99, p=0.01; Tukey HSD p=0.008), whereas MinoKO-CCI mice did not differ from Sham (p=0.6) and differed from Control-CCI mice with marginal significance (p=0.057). MinoKO-CCI mice also show increased locomotor activity in the OFT (p=.009) (Fig. 6H) compared to sham injured mice with no differences observed across all groups in spatial working memory (Fig. 6I). Preliminary analysis of fear conditioning data revealed significant main effects of knockout (irrespective of CCI assignment), thus invalidating a grouping together of sham-control and sham-knockout mice. We instead present here the more basic analysis, using separate model terms for CCI treatment and genotype. The effects of microglial Nogo-KO varied significantly depending on phase of testing (genotype x phase interaction $F_{3,48}$=3.33, p=0.03). Significant differences were found only during the recovery phase on training day, with MinoKO mice freezing more (main effect of genotype $F_{1,16}$=12.58,p=0.003), and CCI-treated mice freezing less ($F_{1,16}$=5.06,p=0.04). This indicates genotype specific

effects, as have been shown before with global Nogo-A knockout (Willi et al., 2010), as well as separate CCI specific effects in the fear conditioning paradigm. Full results of fear conditioning are shown in Figure S1.

Microglial Nogo deletion accelerates symmetrical motor function recovery following CCI

Analysis of EBST prior to CCI found no baseline differences between genotypes ($F_{2,18}$=0.49, p=0.6) or sexes ($F_{1,18}$=0.01, p=0.9) (Fig. 7B). For analysis with respect to CCI treatment, mice were re-assigned to one of three groups: Sham (including all three genotypes), Control-CCI (including Floxed Control and Cre Control) and MinoKO-CCI . Linear mixed effects analysis of all three time points (baseline, 7 and 14 days post-CCI) revealed that the consequences of CCI treatment depended on timing (significant CCI group x date interaction $F_{4,36}$=3.63, p=0.01). Individual linear model analyses for each test date identified significant CCI group differences only at the 7d post-CCI time point ($F_{2,18}$=8.36, p=0.003) (Fig. 7C), with Tukey's post-hoc comparisons revealing differences between groups (p=.0012 for Sham v. CCI-Control and p=.0090 for Control-CCI v. MinoKO-CCI). There was much higher variability at the 14-day timepoint (Fig. 7D), which may have been a consequence, in part, of the behavioral tests taking place between these timepoints.

Discussion

TBI is a leading cause of global mortality. For those who survive, it can be debilitating both immediately afterward as well as and for years following, especially in individuals who suffer repeated head injury (Glotfelty et al., 2019). There is currently a void of drugs available for treating TBI, which presents an urgency to understand TBI injury mechanisms and potential targets for intervention. Neuroinflammation accompanies the initial TBI but can persist chronically for years following a single injury. The process of neuroinflammation is a key component of the brain's primary defense mechanism and is not wholly pathological (DiSabato et al., 2016); however, chronic or excessively high levels of inflammatory proteins can exacerbate damage and produce a secondary injury, which has been linked to accelerated neurodegeneration and chronic traumatic encephalopathy (Simon et al., 2017).The present study, importantly, demonstrates a key role of the Nogo signaling system within microglia-associated neuroinflammation by evaluating the selective deletion of Nogo in microglia through the generation of MinoKO mice during health and an acute inflammatory challenge, namely moderate TBI. Whereas MinoKO and Control mice were indistinguishable in relation to their microglial morphology in uninjured brain and behavior during health, microglial Nogo deletion supported initiation of a compensatory brain inflammatory response following TBI challenge but moderated microglial cell activation. This was evident by a more subdued elevation in Iba1+ and GFAP+ cells in the cortical and thalamic regions adjacent to TBI, measures associated with phenotypic changes in microglia relating to their activation status, and time-dependent measures of behavioral activity post TBI.

The Nogo signaling system may be a potential target for treating TBI, as it is inhibitory for neurite outgrowth, promotes growth cone collapse of neurons, prevents CNS repair following injury (Schwab and Strittmatter, 2014), and recently, has been linked to the

regulation of inflammation (Zhang et al., 2022). The three Nogo protein isoforms, Nogo-A, -B, and -C signal through the Nogo-66 receptor (NgR1). Germline deletion of Nogo-A, Nogo-A and -B, or Nogo-A, -B, and -C have mixed results in influencing axonal regeneration following spinal cord injury (SCI) (Kim et al., 2003; Simonen et al., 2003; Zheng et al., 2003). NgR1 deletion or inhibition has similarly had mixed results influencing recovery from injury, including TBI (GrandPré et al., 2002; Lee et al., 2004; Tong et al., 2013; Zheng et al., 2005). In a mouse model of mild-TBI, which represents the severity of a majority of human TBI injuries, upregulation of the Nogo-66 receptor in neurons aggravated the effects of the injury and increased the amount of time needed for recovery (Lai et al., 2018). Cell-type specific roles of Nogo protein have been explored, with deletion in oligodendrocytes contributing to axonal repair and improved functional outcomes more than deletion in neurons (Meves et al., 2018; Vajda et al., 2015). Neuronal and oligodendrocyte specific Nogo also differentially restrict synaptic plasticity (Zemmar et al., 2017). Meves et al. (2018) (Meves et al., 2018) designed a floxed Nogo mouse similar to a previously used mouse with constitutive deletion of the first exon common to Nogo-A, -B, and -C, which resulted in null or hypomorph expression of all three proteins (Zheng et al., 2003). Their mouse, and the MinoKO mice used in the current studies, however, includes the deletion of the first and second exon common to all three Nogo isoforms of Nogo, representing perhaps even more enhanced knock out model (Meves et al., 2018). Although there is a possibility for compensatory expression of Nogo in other cell types, it is unlikely due to the targeted nature of the Cre-LoxP knockout system and previous results reported in Meves et. al (2018). Future research can certainly address whether compensatory expression of Nogo is occurring in other cell types.

Regardless of this possibility, ours and other groups' research *does* indicate that cell-type specific expression of Nogo protein produces functional differences in pathological contexts. This may also include Nogo expressed on microglia, the immune cells of the brain responsible for initiating a compensatory inflammatory response following injury to instigate repair and ultimately re-achieve homeostasis. As has been demonstrated with other signaling molecules, the same gene or pathway playing multiple roles different cell types is an emerging theme in regulation of CNS injury and repair, with microglia being no exception (Jin and Zheng, 2019; Zheng and Tuszynski, 2023). Microglia are heterogeneous and respond to aberrant signaling or damage by performing a variety of roles. These include phagocytosis of debris or damaged tissue, secretion of proteins including pro-inflammatory cytokines and trophic factors, synaptic pruning, and recruitment of other cells, such as astrocytes, to respond to damage (Amor et al., 2022). Until the current study, microglial-Nogo has not been assessed independently in any rodent injury model.

Here, we utilized the MinoKO mouse to assess the roles of microglial Nogo in healthy and pathological conditions. The MinoKO mouse allows for inducible microglia-specific gene deletion of all three Nogo protein isoforms (Nogo-A, -B, and -C). Using a CCI model of TBI, we induced moderate injury that generates a robust inflammatory response, as we have previously shown (Greig et al., 2019; Hsueh et al., 2022). Nogo initiates the RhoA/ROCK signaling pathway and has been shown to exacerbate inflammation in the presence of a liposaccharide challenge (Glotfelty et al., 2023); it also disrupts adhesion and migration of microglia (Yan et al., 2012). It is possible for Nogo to activate NgR1 on the

same cell (Vajda et al., 2015), which may occur in microglia as they appear responsive to Nogo-66 (Fang et al., 2015; Glotfelty et al., 2023) and clearly express Nogo as we have shown (Fig. 1). Microglia represent a range of phenotypes in pathological contexts, but their distribution and morphologies provide insights to the levels of inflammation in the brain. We found reductions in Iba1 microglial immunoreactivity in the ipsilateral cortex and thalamus of CCI injured MinoKO mice compared to CCI controls (Fig. 4), suggesting that microglial Nogo may reduce the 1) recruitment of microglia to injured areas, 2) the rate of microglial proliferation, or 3) the infiltration of microglial progenitors from the blood to the brain, all of which are common during brain injury (Ladeby et al., 2005). Thalamic microglial activation results from damage sustained to thalamocortical tracts from TBI (Ramlackhansingh et al., 2011; Scott et al., 2015). Interestingly, mice lacking Nogo-B show decreased macrophage infiltration into ischemic limb injury sites, with macrophages showing defects in spreading and migration (Yu et al., 2009). This may partially explain the decreased microgliosis we show here in MinoKO mice.

Concurrently and in response to signaling from microglia during injury, astrocytes also participate in the inflammatory response through a variety of changes, including proliferation and formation of an astrocytic scar in more severe injuries (Burda et al., 2016; Liddelow et al., 2017).We show here reductions of GFAP immunoreactivity in the ipsilateral cortex of CCI injured MinoKO mice compared to CCI and sham control animals. No differences in microglial or astrocytic immunoreactivity were observed in contralateral brain hemispheres between sham or injured animals. Although the reduction in astrocyte reactivity was not as pronounced as the cortical microglial reactivity reductions, these data represent overall reductions in inflammatory environment from Nogo deletion in microglia. Additionally, our data are in line with previous studies suggesting Nogo/NgR1 signaling may affect the migration of microglia to an injury site (Yan et al., 2012; Yu et al., 2009).

Microglia respond context-dependently to cues, with changes in morphology being one of the most obvious indicators of their responding to injury or other non-homeostatic signaling. In a healthy brain, microglia are relatively evenly distributed in a brain region- and age-dependent manner (Moca et al., 2022), and are often referred to as functionally homeostatic. These highly complex cells are characterized by their highly ramified structure defined by many branches emanating from the soma. Upon sensing damage or aberrant signaling cues, microglia become reactive and decrease ramification/branch complexity. In highly pathological contexts, such as moderate TBI (Morrison et al., 2017), microglia retract nearly all branches present as an ameboid shape. Rounder microglia are generally the most highly reactive and are associated with a highly pro-inflammatory environment (Karperien et al., 2013). Previously, work has shown that Nogo protein can affect microglial morphology in the context of TBI (Ziebell et al., 2017), and Nogo-A (Arif Ullah et al., 2021) and Nogo-B (Zhu et al., 2017) facilitate proinflammatory cytokine production typical of reactive microglia. Using *MotiQ* software to assess microglial morphologies two weeks post-CCI, we found microglia from injured MinoKO mice show increased complexity in both the cortex and thalamus compared to injured controls. MinoKO-CCI microglial ramification, spanned area, number of endpoints, and total tree length all trended towards sham injured microglia measures. Microglia from female mice displayed some differences with males, including less overall Iba1 coverage, more ipsilateral cortical endpoints, and

longer ipsilateral cortical total tree length (Tables S1 and S2). Less reactive and more complex female microglia are in line with previous studies describing microglial sex differences, some of which suggest female microglia are less reactive to insult and provide enhanced neuroprotection than male microglia during these insults (Hinkle et al., 2019; Villa et al., 2018). Combined with the microglia and astrocyte coverage measures, the increased overall complexity of MinoKO microglia, regardless of sex, is further evidence of a dampened inflammatory environment.

Behaviorally, healthy MinoKO mice do not differ from control mice when assessed under a variety of motor and cognitive tests, in line with a previous study characterizing behavior, Nogo-A deficient mice showed a similar lack of differences in OFT, EPM, and MWM, among others, compared to control (wild type) mice (Willi et al., 2009). All CCI-injured mice in our study show increased activity compared to pre-TBI conditions, which has previously been described (Bajwa et al., 2016; Tucker et al., 2017); however, CControl-CCI mice were hypoactive compared to both Sham and MinoKO (CCI) mice 24 h after CCI. Meta-analyses show patients with TBI experience higher rates of attention deficit hyperactivity disorder (ADHD) diagnosis than those without such injury (Adeyemo et al., 2014; Asarnow et al., 2021), highlighting similarities between our mouse model and the human injury. TBI-induced activity increases and stereotopy, interpreted as reward salience or underappreciation of rewarding behavior, has been associated with the significant reductions in endocannabinoids observed in the TBI-injured mice (Vogel et al., 2020). Interestingly, blocking enzymes that metabolize cannabinoids attenuates CCI induced behavioral deficits and inflammation (Selvaraj et al., 2019; Tchantchou et al., 2014).

In the Nogo-A deficient mice, Willi et al. (2009) (Willi et al., 2009) showed increased motor control in the accelerating rotorod task along with increased overall spontaneous dark phase activity. In this and another follow up study, Nogo-A deficient mice show significantly increased hyperactivity from an amphetamine challenge compared to control mice (Willi et al., 2010). Although a majority of our behavioral assays detected no differences between healthy control and MinoKO mice (Fig. 2), injured MinoKO mice show significantly increased dark phase activity immediately following CCI compared to sham and injury controls. CCI injured MinoKO mice also increase distance traveled in the OFT ~1 week post CCI (Fig. 6), in line with the described amphetamine challenges above. Nogo-A knock-down (KD) in rats affected circadian rhythmicity, reducing overall activity when the animals were in constant darkness but not in normal 12 hour light-12 hour dark cycles (Petrasek et al., 2014). This effect is opposite to that observed in healthy and unchallenged mice from Willi et al. (2009) (Willi et al., 2009). Although all of the described previous studies and ours are very different, a common thread emerges that Nogo-A may be involved in regulating daily patterns of activity. Notably, circadian rhythm is disrupted in TBI patients (Grima et al., 2016) and rodents (Korthas et al., 2022) which is perhaps aggravated by Nogo-A deficiency.

Our studies imply that, at least in pathological conditions, microglial Nogo-A deficiency may largely be responsible for observed activity increases seen across the above described studies. In addition, the relatively short period, weeks rather than months, of Nogo deletion in MinoKO mice and KD rats compared to the constitutively deleted Nogo in the other

studies suggests this effect involves rapid neurochemical changes in the brain rather than structural changes which occur on longer timescales. In Willi et al. (2010) (Willi et al., 2010), researchers found decreased serotonin and its metabolites in the striatum and region-specific up- and down-regulation of dopamine receptors throughout the brain. Dopamine turnover was increased in the prefrontal cortex, while serotonin turnover was reduced in the striatum. Another study in Nogo deficient mice detected increased levels of serotonin in the prefrontal cortex, with no differences in dopamine observed (Enkel et al., 2014). Moreover, with increasing age, humans show increased Nogo-A expression within the dopaminergic rich substantia nigra, while the opposite is true for PD patients (Eyer et al., 2021). Neurochemical imbalances caused by lack of Nogo protein may be involved in the hyperactivity observed across studies in Nogo-A KO or KD mice.

In addition to the increased locomotion phenotype, Willi et al. (2010) (Willi et al., 2010) observed increased freezing in Nogo deficient mice, but only when animals had been pre-exposed to a conditioning environment. Our results in a more traditional (no pre-exposure) paradigm indicate a reduction in freezing after CCI regardless of genotype; however, we also show a genotype effect of increased freezing in MinoKO mice. This result indicates that microglial Nogo deficiency in adult mice is sufficient to produce the increased freezing effect that was undetected in lifelong Nogo-A deficient mice (Willi et al., 2010). Willi et al. (2010) also provide evidence with Nogo-A antibody studies that lifelong lack of Nogo-A is required for the behavioral phenotypes observed, contrary to our findings. Perhaps KO of all three Nogo isoforms in microglia produces the behavioral effect that was not achievable with antibodies alone.

An additional piece of evidence that microglial Nogo delays recovery in the CCI injury model comes from results on the elevated body swing test (EBST), which measures asymmetrical motor function typical from unilateral brain lesions (Borlongan et al., 1995). Using this method, uninjured animals show no biased swing activity when supported by the tail; however, CCI injured mice show significant biased swing contralateral to injury 7 days and up to two weeks post CCI. This biased contralateral swing is mitigated using anti-inflammatory drugs as we have previously shown (Hsueh et al., 2019). MinoKO-CCI mice show no differences between sham injured controls either 7 or 14 days post CCI, while the CCI control mice show significant contralateral biased swing at 7 days post CCI. MinoKO-CCI mice display similar levels of home cage activity as Sham injured animals several days after injury, while Control-CCI mice were significantly less active. This supports our finding that microglial Nogo deletion facilitates recovery and is in line with the EBST improvements observed in MinoKO-CCI mice. Our evidence of reduced inflammatory load in the MinoKO mouse brain as well as decreased enlargement of the ipsilateral lateral ventricle is in line with the resolution of asymmetrical motor control that we see by pharmacologically disrupting inflammation and, in this light, Nogo presence on microglia represents a putative drug target to mitigate neuroinflammation (Glotfelty et al., 2023). Although, CCI injured Control and MinoKO mice showed similar levels of tissue loss indicated from the Giemsa staining, future studies should assess viable tissue via 2,3,5-triphenyltetrazolium chloride (TTC), as has previously been done with the CCI model (Farr et al., 2020). Others have detected differences in mouse behavior and pathology from Cx3Cr1 heterozygosity (Corona et al., 2010; Rogers et al., 2011), we are confident

our results represent effects of microglial Nogo deletion as the wildtype Cx3Cr1 expressing mice (Floxed controls) and Cre Control mice did not exhibit major phenotype differences.

This is the first microglial specific Nogo KO mouse model and adds to the growing evidence that Nogo may play cell-type specific roles. Previous work suggests preservation of Nogo protein in neurons with deletion in oligodendrocytes, the myelinating glia of the brain, promotes axonal repair (Meves et al., 2018; Vajda et al., 2015). Our studies add to these findings as neuronal Nogo remains intact in the MinoKO mice. A microglial specific NgR1-KO mouse subject to a pathological condition would provide interesting context to our studies. Further characterization of microglial transcriptomes from MinoKO mice would provide even more evidence for the roles that Nogo-A, -B, and -C have on inflammation in the brain. Interest in Nogo protein influence on the inflammation process and our studies confirm that further work is needed to characterize this multifaceted protein family previously only described for neurite growth restricting properties.

Supplementary Material

Refer to Web version on PubMed Central for supplementary material.

Acknowledgements

The authors thank Dr. Aaron McGee, University of Louisville, for providing the initial breeding mice for our studies. All graphics related to the manuscript were created using BioRender.com.

Funding

The research of the authors was supported in part by (i) the Intramural Research Program of the National Institute on Aging, National Institutes of Health, USA (AG00000994) (E.J.G., S.C.H., Q.C., D.T., K.O.K., R.M., T.W., N.H.G.) (ii) the Swedish Research Council K2012-62X-03185-42-4 (L.O., T.E.K., E.J.G.), (iii) the Swedish Brain Foundation (L.O., T.E.K., E.J.G.), (iv) NIH grant NS093055 (B.Z.), (v) NIH grants R01NS127074, R01NS107365, R21NS127177 (Y.L.), and (vi.) NIH 1F31NS125930-01 (A.B.). E.J.G is supported by the NIH-Karolinska Institutet Graduate Partnership Program.

Data Availability

The data that support the findings of this study are available from the corresponding author upon reasonable request.

References

Adeyemo BO, Biederman J, Zafonte R, Kagan E, Spencer TJ, Uchida M, Kenworthy T, Spencer AE, Faraone SV, 2014. Mild Traumatic Brain Injury and ADHD: A Systematic Review of the Literature and Meta-Analysis. J. Atten. Disord 10.1177/1087054714543371

Amor S, McNamara NB, Gerrits E, Marzin MC, Kooistra SM, Miron VE, Nutma E, 2022. White matter microglia heterogeneity in the CNS. Acta Neuropathol. 10.1007/s00401-021-02389-x

Arif Ullah HM, Elfadl AK, Park S, Kim YD, Chung MJ, Son JY, Yun HH, Park JM, Yim JH, Jung SJ, Choi YC, Shin JH, Kim DS, Park JK, Jeong KS, 2021. Nogo-A is critical for pro-inflammatory gene regulation in myocytes and macrophages. Cells 10, 1–20. 10.3390/cells10020282

Asarnow RF, Newman N, Weiss RE, Su E, 2021. Association of attention-deficit/hyperactivity disorder diagnoses with pediatric traumatic brain injury: A meta-analysis. JAMA Pediatr. 10.1001/jamapediatrics.2021.2033

Bajwa NM, Halavi S, Hamer M, Semple BD, Noble-Haeusslein LJ, Baghchechi M, Hiroto A, Hartman RE, Obenaus A, 2016. Mild concussion, but not moderate traumatic brain injury, is associated with long-term depression-like phenotype in mice. PLoS One 11, e0146886. 10.1371/journal.pone.0146886 [PubMed: 26796696]

Bandtlow CE, Dlaska M, Pirker S, Czech T, Baumgartner C, Sperk G, 2004. Increased expression of Nogo-A in hippocampal neurons of patients with temporal lobe epilepsy. Eur. J. Neurosci 20, 195–206. 10.1111/j.1460-9568.2004.03470.x [PubMed: 15245492]

Baya Mdzomba J, Joly S, Rodriguez L, Dirani A, Lassiaz P, Behar-Cohen F, Pernet V, 2020. Nogo-A-targeting antibody promotes visual recovery and inhibits neuroinflammation after retinal injury. Cell Death Dis. 11, 1–16. 10.1038/s41419-020-2302-x [PubMed: 31911576]

Bedolla AM, McKinsey G, Ware K, Santander N, Arnold T, Luo Y, 2023. Finding the right tool: a comprehensive evaluation of microglial inducible cre mouse models. bioRxiv 2023.04.17.536878. 10.1101/2023.04.17.536878

Borlongan CV, Randall TS, Cahill DW, Sanberg PR, 1995. Asymmetrical motor behavior in rats with unilateral striatal excitotoxic lesions as revealed by the elevated body swing test. Brain Res. 676, 231–234. 10.1016/0006-8993(95)00150-O [PubMed: 7796175]

Burda JE, Bernstein AM, Sofroniew MV, 2016. Astrocyte roles in traumatic brain injury. Exp. Neurol 10.1016/j.expneurol.2015.03.020

Cardona SM, Mendiola AS, Yang YC, Adkins SL, Torres V, Cardona AE, 2015. Disruption of fractalkine signaling leads to microglial activation and neuronal damage in the diabetic retina. ASN Neuro 7. 10.1177/1759091415608204

Corona AW, Huang Y, O'Connor JC, Dantzer R, Kelley KW, Popovich PG, Godbout JP, 2010. Fractalkine receptor (CX3CR1) deficiency sensitizes mice to the behavioral changes induced by lipopolysaccharide. J. Neuroinflammation 7, 1–14. 10.1186/1742-2094-7-93 [PubMed: 20047691]

Dickendesher TL, Baldwin KT, Mironova YA, Koriyama Y, Raiker SJ, Askew KL, Wood A, Geoffroy CG, Zheng B, Liepmann CD, Katagiri Y, Benowitz LI, Geller HM, Giger RJ, 2012. NgR1 and NgR3 are receptors for chondroitin sulfate proteoglycans. Nat. Neurosci 15, 703–712. 10.1038/nn.3070 [PubMed: 22406547]

Dimou L, Schnell L, Montani L, Duncan C, Simonen M, Schneider R, Liebscher T, Gullo M, Schwab ME, 2006. Nogo-A-deficient mice reveal strain-dependent differences in axonal regeneration. J. Neurosci 26, 5591–603. 10.1523/JNEUROSCI.1103-06.2006 [PubMed: 16723516]

DiSabato DJ, Quan N, Godbout JP, 2016. Neuroinflammation: the devil is in the details. J. Neurochem 139, 136–153. 10.1111/jnc.13607 [PubMed: 26990767]

Donat CK, Gaber K, Meixensberger J, Brust P, Pinborg LH, Hansen HH, Mikkelsen JD, 2016. Changes in Binding of [123I]CLINDE, a High-Affinity Translocator Protein 18 kDa (TSPO) Selective Radioligand in a Rat Model of Traumatic Brain Injury. NeuroMolecular Med. 18, 158–169. 10.1007/s12017-016-8385-y [PubMed: 26969181]

Enkel T, Berger SM, Schönig K, Tews B, Bartsch D, 2014. Reduced expression of Nogo-A leads to motivational deficits in rats. Front. Behav. Neurosci 8, 10. 10.3389/fnbeh.2014.00010 [PubMed: 24478657]

Eyer GC, Di Santo S, Hewer E, Andereggen L, Seiler S, Widmer HR, 2021. Co-expression of nogo-a in dopaminergic neurons of the human substantia nigra pars compacta is reduced in parkinson's disease. Cells 10, 3368. 10.3390/cells10123368 [PubMed: 34943877]

Fang Y, Yan J, Li C, Zhou X, Yao L, Pang T, Yan M, Zhang L, Mao L, Liao H, 2015. The Nogo/Nogo Receptor (NgR) Signal Is Involved in Neuroinflammation through the Regulation of Microglial Inflammatory Activation. J. Biol. Chem 290, 28901–14. 10.1074/jbc.M115.678326 [PubMed: 26472924]

Farr SA, Cuzzocrea S, Esposito E, Campolo M, Niehoff ML, Doyle TM, Salvemini D, 2020. Adenosine A3 receptor as a novel therapeutic target to reduce secondary events and improve neurocognitive functions following traumatic brain injury. J. Neuroinflammation 17, 339. 10.1186/s12974-020-02009-7 [PubMed: 33183330]

File SE, 1993. The interplay of learning and anxiety in the elevated plus-maze. Behav. Brain Res 58, 199–202. 10.1016/0166-4328(93)90103-w [PubMed: 8136046]

Gil V, Nicolas O, Mingorance A, Ureña JM, Tang BL, Hirata T, Sáez-Valero J, Ferrer I, Soriano E, Del Río JA, 2006. Nogo-A expression in the human hippocampus in normal aging and in Alzheimer disease. J. Neuropathol. Exp. Neurol 65, 433–444. 10.1097/01.jnen.0000222894.59293.98 [PubMed: 16772867]

Glotfelty EJ, Delgado TE, Tovar-y-Romo LB, Luo Y, Hoffer BJ, Olson L, Karlsson TE, Mattson MP, Harvey BK, Tweedie D, Li Y, Greig NH, 2019. Incretin Mimetics as Rational Candidates for the Treatment of Traumatic Brain Injury. ACS Pharmacol. Transl. Sci 2, 66–91. 10.1021/acsptsci.9b00003 [PubMed: 31396586]

Glotfelty EJ, Tovar-y-Romo LB, Hsueh S-C, Tweedie D, Li Y, Harvey BK, Hoffer BJ, Karlsson TE, Olson L, Greig NH, 2023. The RhoA-ROCK1/ROCK2 Pathway Exacerbates Inflammatory Signaling in Immortalized and Primary Microglia. Cells 12, 1367. 10.3390/CELLS12101367 [PubMed: 37408199]

Gonzenbach RR, Schwab ME, 2008. Disinhibition of neurite growth to repair the injured adult CNS: Focusing on Nogo. Cell. Mol. Life Sci 10.1007/s00018-007-7170-3

GrandPré T, Shuxin LI, Strittmatter SM, 2002. Nogo-66 receptor antagonist peptide promotes axonal regeneration. Nature 417, 547–551. 10.1038/417547a [PubMed: 12037567]

Greig NH, Lecca D, Hsueh SC, Nogueras-Ortiz C, Kapogiannis D, Tweedie D, Glotfelty EJ, Becker RE, Chiang YH, Hoffer BJ, 2019. (−)-Phenserine tartrate (PhenT) as a treatment for traumatic brain injury. CNS Neurosci. Ther. cns13274. 10.1111/cns.13274

Grima NA, Ponsford JL, St Hilaire MA, Mansfield D, Rajaratnam SM, 2016. Circadian Melatonin Rhythm Following Traumatic Brain Injury. Neurorehabil. Neural Repair 30, 972–977. 10.1177/1545968316650279 [PubMed: 27221043]

Hammond TR, Dufort C, Dissing-Olesen L, Giera S, Young A, Wysoker A, Walker AJ, Gergits F, Segel M, Nemesh J, Marsh SE, Saunders A, Macosko E, Ginhoux F, Chen J, Franklin RJM, Piao X, McCarroll SA, Stevens B, 2019. Single-Cell RNA Sequencing of Microglia throughout the Mouse Lifespan and in the Injured Brain Reveals Complex Cell-State Changes. Immunity 50, 253–271.e6. 10.1016/j.immuni.2018.11.004 [PubMed: 30471926]

Heras-Romero Y, Morales-Guadarrama A, Santana-Martínez R, Ponce I, Rincón-Heredia R, Poot-Hernández AC, Martínez-Moreno A, Urrieta E, Bernal-Vicente BN, Campero-Romero AN, Moreno-Castilla P, Greig NH, Escobar ML, Concha L, Tovar-y-Romo LB, 2022. Improved post-stroke spontaneous recovery by astrocytic extracellular vesicles. Mol. Ther 30, 798–815. 10.1016/j.ymthe.2021.09.023 [PubMed: 34563674]

Hinkle JJ, Olschowka JA, Love TM, Williams JP, O'Banion MK, 2019. Cranial irradiation mediated spine loss is sex-specific and complement receptor-3 dependent in male mice. Sci. Rep 9, 18899. 10.1038/s41598-019-55366-6 [PubMed: 31827187]

Hsueh SC, Lecca D, Greig NH, Wang JY, Selman W, Hoffer BJ, Miller JP, Chiang YH, 2019. (−)-Phenserine Ameliorates Contusion Volume, Neuroinflammation, and Behavioral Impairments Induced by Traumatic Brain Injury in Mice. Cell Transplant. 28, 1183–1196. 10.1177/0963689719854693 [PubMed: 31177840]

Hsueh SC, Luo W, Tweedie D, Kim DS, Kim YK, Hwang I, Gil JE, Han BS, Chiang YH, Selman W, Hoffer BJ, Greig NH, 2021. N-Adamantyl Phthalimidine: A New Thalidomide-like Drug That Lacks Cereblon Binding and Mitigates Neuronal and Synaptic Loss, Neuroinflammation, and Behavioral Deficits in Traumatic Brain Injury and LPS Challenge. ACS Pharmacol. Transl. Sci 4, 980–1000. 10.1021/acsptsci.1c00042 [PubMed: 33860215]

Hsueh SC, Scerba MT, Tweedie D, Lecca D, Kim DS, Baig AM, Kim YK, Hwang I, Kim S, Selman WR, Hoffer BJ, Greig NH, 2022. Activity of a Novel Anti-Inflammatory Agent F-3,6′-dithiopomalidomide as a Treatment for Traumatic Brain Injury. Biomedicines 10, 2449. 10.3390/biomedicines10102449 [PubMed: 36289711]

Hughes RN, 2007. Neotic preferences in laboratory rodents: Issues, assessment and substrates. Neurosci. Biobehav. Rev 10.1016/j.neubiorev.2006.11.004

Jawhar S, Trawicka A, Jenneckens C, Bayer TA, Wirths O, 2012. Motor deficits, neuron loss, and reduced anxiety coinciding with axonal degeneration and intraneuronal Aβ aggregation in the 5XFAD mouse model of Alzheimer's disease. Neurobiol. Aging 33, 196.e29–196.e40. 10.1016/j.neurobiolaging.2010.05.027

Jin Y, Zheng B, 2019. Multitasking: Dual leucine zipper-bearing kinases in neuronal development and stress management. Annu. Rev. Cell Dev. Biol 10.1146/annurev-cellbio-100617-062644

Karlén A, Karlsson TE, Mattsson A, Lundströmer K, Codeluppi S, Pham TM, Bäckman CM, Ogren SO, Aberg E, Hoffman AF, Sherling MA, Lupica CR, Hoffer BJ, Spenger C, Josephson A, Brené S, Olson L, Karlen A, Lundstromer K, Backman CM, Brene S, 2009. Nogo receptor 1 regulates formation of lasting memories. Proc. Natl. Acad. Sci 106, 20476–20481. 10.1073/pnas.0905390106 [PubMed: 19915139]

Karlsson TE, Smedfors G, Brodin ATS, Aberg E, Mattsson A, Högbeck I, Wellfelt K, Josephson A, Brené S, Olson L, 2016. NgR1: A Tunable Sensor Regulating Memory Formation, Synaptic, and Dendritic Plasticity. Cereb. Cortex 26, 1804–1817. 10.1093/cercor/bhw007 [PubMed: 26838771]

Karperien A, Ahammer H, Jelinek HF, 2013. Quantitating the subtleties of microglial morphology with fractal analysis. Front. Cell. Neurosci 10.3389/fncel.2013.00003

Kim JE, Li S, Grand Pré T, Qiu D, Strittmatter SM, 2003. Axon regeneration in young adult mice lacking Nogo-A/B. Neuron 38, 187–199. 10.1016/S0896-6273(03)00147-8 [PubMed: 12718854]

Kloss CU, Bohatschek M, Kreutzberg GW, Raivich G, 2001. Effect of lipopolysaccharide on the morphology and integrin immunoreactivity of ramified microglia in the mouse brain and in cell culture. Exp. Neurol 168, 32–46. 10.1006/exnr.2000.7575 [PubMed: 11170719]

Konhilas JP, Chen H, Luczak E, McKee LA, Regan J, Watson PA, Stauffer BL, Khalpey ZI, McKinsey TA, Horn T, LaFleur B, Leinwand LA, 2015. Diet and sex modify exercise and cardiac adaptation in the mouse. Am. J. Physiol. - Hear. Circ. Physiol 308, H135–H145. 10.1152/ajpheart.00532.2014

Korthas HT, Main BS, Harvey AC, Buenaventura RG, Wicker E, Forcelli PA, Burns MP, 2022. The Effect of Traumatic Brain Injury on Sleep Architecture and Circadian Rhythms in Mice—A Comparison of High-Frequency Head Impact and Controlled Cortical Injury. Biology (Basel). 11, 1031. 10.3390/biology11071031 [PubMed: 36101412]

Ladeby R, Wirenfeldt M, Garcia-Ovejero D, Fenger C, Dissing-Olesen L, Dalmau I, Finsen B, 2005. Microglial cell population dynamics in the injured adult central nervous system, in: Brain Research Reviews. Elsevier, pp. 196–206. 10.1016/j.brainresrev.2004.12.009

Lai J-H, Karlsson TE, Wu JC-C, Huang C-Z, Chen Y-H, Kang S-J, Brodin ATS, Hoffer BJ, Olson L, Chiang Y-H, Chen K-Y, 2018. Role of Nogo Receptor-1 for Recovery of Balance, Cognition, and Emotion after Mild Traumatic Brain Injury in Mice. J. Neurotrauma neu2018.5949. 10.1089/neu.2018.5949

Lecca D, Jung YJ, Scerba MT, Hwang I, Kim YK, Kim S, Modrow S, Tweedie D, Hsueh SC, Liu D, Luo W, Glotfelty E, Li Y, Wang JY, Luo Y, Hoffer BJ, Kim DS, McDevitt RA, Greig NH, 2022. Role of chronic neuroinflammation in neuroplasticity and cognitive function: A hypothesis. Alzheimer's Dement. 18, 2327–2340. 10.1002/alz.12610 [PubMed: 35234334]

Lee J-K, Kim J-E, Sivula M, Strittmatter SM, 2004. Nogo Receptor Antagonism Promotes Stroke Recovery by Enhancing Axonal Plasticity. J. Neurosci 24.

Lee JK, Geoffroy CG, Chan AF, Tolentino KE, Crawford MJ, Leal MA, Kang B, Zheng B, 2010. Assessing Spinal Axon Regeneration and Sprouting in Nogo-, MAG-, and OMgp-Deficient Mice. Neuron 66, 663–670. 10.1016/j.neuron.2010.05.002 [PubMed: 20547125]

Levin HS, Meyers CA, Grossman RG, Sarwar M, 1981. Ventricular Enlargement After Closed Head Injury. Arch. Neurol 38, 623–629. 10.1001/archneur.1981.00510100051007 [PubMed: 6975095]

Liddelow SA, Guttenplan KA, Clarke LE, Bennett FC, Bohlen CJ, Schirmer L, Bennett ML, Münch AE, Chung WS, Peterson TC, Wilton DK, Frouin A, Napier BA, Panicker N, Kumar M, Buckwalter MS, Rowitch DH, Dawson VL, Dawson TM, Stevens B, Barres BA, 2017. Neurotoxic reactive astrocytes are induced by activated microglia. Nature 541, 481–487. 10.1038/nature21029 [PubMed: 28099414]

Madry C, Kyrargyri V, Arancibia-Cárcamo IL, Jolivet R, Kohsaka S, Bryan RM, Attwell D, 2018. Microglial Ramification, Surveillance, and Interleukin-1β Release Are Regulated by the Two-Pore Domain K(+) Channel THIK-1. Neuron 97, 299–312.e6. 10.1016/j.neuron.2017.12.002 [PubMed: 29290552]

Masliah E, Xie F, Dayan S, Rockenstein E, Mante M, Adame A, Patrick CM, Chan AF, Zheng B, 2010. Genetic deletion of Nogo/Rtn4 ameliorates behavioral and neuropathological

outcomes in amyloid precursor protein transgenic mice. Neuroscience 169, 488–494. 10.1016/j.neuroscience.2010.04.045 [PubMed: 20433905]

Meves JM, Geoffroy CG, Kim ND, Kim JJ, Zheng B, 2018. Oligodendrocytic but not neuronal Nogo restricts corticospinal axon sprouting after CNS injury. Exp. Neurol 309, 32–43. 10.1016/j.expneurol.2018.07.013 [PubMed: 30055160]

Moca EN, Lecca D, Hope KT, Etienne F, Schaler AW, Espinoza K, Chappell MS, Gray DT, Tweedie D, Sidhu S, Masukawa L, Sitoy H, Mathew R, Saban DR, Greig NH, De Biase LM, 2022. Microglia Drive Pockets of Neuroinflammation in Middle Age. J. Neurosci 42, 3896–3918. 10.1523/JNEUROSCI.1922-21.2022 [PubMed: 35396327]

Morris R, 1984. Developments of a water-maze procedure for studying spatial learning in the rat. J. Neurosci. Methods 11, 47–60. 10.1016/0165-0270(84)90007-4 [PubMed: 6471907]

Morrison H, Young K, Qureshi M, Rowe RK, Lifshitz J, 2017. Quantitative microglia analyses reveal diverse morphologic responses in the rat cortex after diffuse brain injury. Sci. Rep 7, 1–12. 10.1038/s41598-017-13581-z [PubMed: 28127051]

Novak G, Kim D, Seeman P, Tallerico T, 2002. Schizophrenia and Nogo: Elevated mRNA in cortex, and high prevalence of a homozygous CAA insert. Mol. Brain Res 107, 183–189. 10.1016/S0169-328X(02)00492-8 [PubMed: 12425946]

Oydanich M, Babici D, Zhang J, Rynecki N, Vatner DE, Vatner SF, 2019. Mechanisms of sex differences in exercise capacity. Am. J. Physiol. - Regul. Integr. Comp. Physiol 316, R832–R838. 10.1152/ajpregu.00394.2018 [PubMed: 31017810]

Paolicelli RC, Sierra A, Stevens B, Tremblay ME, Aguzzi A, Ajami B, Amit I, Audinat E, Bechmann I, Bennett M, Bennett F, Bessis A, Biber K, Bilbo S, Blurton-Jones M, Boddeke E, Brites D, Brône B, Brown GC, Butovsky O, Carson MJ, Castellano B, Colonna M, Cowley SA, Cunningham C, Davalos D, De Jager PL, de Strooper B, Denes A, Eggen BJL, Eyo U, Galea E, Garel S, Ginhoux F, Glass CK, Gokce O, Gomez-Nicola D, González B, Gordon S, Graeber MB, Greenhalgh AD, Gressens P, Greter M, Gutmann DH, Haass C, Heneka MT, Heppner FL, Hong S, Hume DA, Jung S, Kettenmann H, Kipnis J, Koyama R, Lemke G, Lynch M, Majewska A, Malcangio M, Malm T, Mancuso R, Masuda T, Matteoli M, McColl BW, Miron VE, Molofsky AV, Monje M, Mracsko E, Nadjar A, Neher JJ, Neniskyte U, Neumann H, Noda M, Peng B, Peri F, Perry VH, Popovich PG, Pridans C, Priller J, Prinz M, Ragozzino D, Ransohoff RM, Salter MW, Schaefer A, Schafer DP, Schwartz M, Simons M, Smith CJ, Streit WJ, Tay TL, Tsai LH, Verkhratsky A, von Bernhardi R, Wake H, Wittamer V, Wolf SA, Wu LJ, Wyss-Coray T, 2022. Microglia states and nomenclature: A field at its crossroads. Neuron. 10.1016/j.neuron.2022.10.020

Pernold K, Iannello F, Low BE, Rigamonti M, Rosati G, Scavizzi F, Wang J, Raspa M, Wiles MV, Ulfhake B, 2019. Towards large scale automated cage monitoring - Diurnal rhythm and impact of interventions on in-cage activity of C57BL/6J mice recorded 24/7 with a non-disrupting capacitive-based technique. PLoS One 14, e0211063. 10.1371/journal.pone.0211063 [PubMed: 30716111]

Petrasek T, Prokopova I, Sladek M, Weissova K, Vojtechova I, Bahnik S, Zemanova A, Schönig K, Berger S, Tews B, Bartsch D, Schwab ME, Sumova A, Stuchlik A, 2014. Nogo-A-deficient transgenic rats show deficits in highe cognitive functions, decreased anxiety, and altered circadian activity patterns. Front. Behav. Neurosci 8. 10.3389/fnbeh.2014.00090

Radulovic J, Kammermeier J, Spiess J, 1998. Generalization of fear responses in C57BL/6N mice subjected to one-trial foreground contextual fear conditioning. Behav. Brain Res 95, 179–189. 10.1016/s0166-4328(98)00039-4 [PubMed: 9806438]

Ramlackhansingh AF, Brooks DJ, Greenwood RJ, Bose SK, Turkheimer FE, Kinnunen KM, Gentleman S, Heckemann RA, Gunanayagam K, Gelosa G, Sharp DJ, 2011. Inflammation after trauma: Microglial activation and traumatic brain injury. Ann. Neurol 70, 374–383. 10.1002/ana.22455 [PubMed: 21710619]

Rogers JT, Morganti JM, Bachstetter AD, Hudson CE, Peters MM, Grimmig BA, Weeber EJ, Bickford PC, Gemma C, 2011. CX3CR1 deficiency leads to impairment of hippocampal cognitive function and synaptic plasticity. J. Neurosci 31, 16241–16250. 10.1523/JNEUROSCI.3667-11.2011 [PubMed: 22072675]

Rueden CT, Schindelin J, Hiner MC, DeZonia BE, Walter AE, Arena ET, Eliceiri KW, 2017. ImageJ2: ImageJ for the next generation of scientific image data. BMC Bioinformatics 18, 1–26. 10.1186/s12859-017-1934-z [PubMed: 28049414]

Satoh JI, Onoue H, Arima K, Yamamura T, 2005. Nogo-A and Nogo receptor expression in demyelinating lesions of multiple sclerosis. J. Neuropathol. Exp. Neurol 64, 129–138. 10.1093/jnen/64.2.129 [PubMed: 15751227]

Schwab ME, 2010. Functions of Nogo proteins and their receptors in the nervous system. Nat. Rev. Neurosci 11, 799–811. 10.1038/nrn2936 [PubMed: 21045861]

Schwab ME, Strittmatter SM, 2014. Nogo limits neural plasticity and recovery from injury. Curr. Opin. Neurobiol 10.1016/j.conb.2014.02.011

Scott G, Hellyer PJ, Ramlackhansingh AF, Brooks DJ, Matthews PM, Sharp DJ, 2015. Thalamic inflammation after brain trauma is associated with thalamo-cortical white matter damage. J. Neuroinflammation 12, 224. 10.1186/s12974-015-0445-y [PubMed: 26627199]

Selvaraj P, Wen J, Tanaka M, Zhang Y, 2019. Therapeutic Effect of a Novel Fatty Acid Amide Hydrolase Inhibitor PF04457845 in the Repetitive Closed Head Injury Mouse Model. J. Neurotrauma 36, 1655–1669. 10.1089/neu.2018.6226 [PubMed: 30526351]

Simon DW, McGeachy MJ, Baylr H, Clark RSB, Loane DJ, Kochanek PM, 2017. The far-reaching scope of neuroinflammation after traumatic brain injury. Nat. Rev. Neurol 10.1038/nrneurol.2017.13

Simonen M, Pedersen V, Weinmann O, Schnell L, Buss A, Ledermann B, Christ F, Sansig G, Van Der Putten H, Schwab ME, 2003. Systemic deletion of the myelin-associated outgrowth inhibitor Nogo-A improves regenerative and plastic responses after spinal cord injury. Neuron 38, 201–211. 10.1016/S0896-6273(03)00226-5 [PubMed: 12718855]

Tchantchou F, Tucker LB, Fu AH, Bluett RJ, McCabe JT, Patel S, Zhang Y, 2014. The fatty acid amide hydrolase inhibitor PF-3845 promotes neuronal survival, attenuates inflammation and improves functional recovery in mice with traumatic brain injury. Neuropharmacology 85, 427–439. 10.1016/j.neuropharm.2014.06.006 [PubMed: 24937045]

Thallmair M, Metz GAS, Z'Graggen WJ, Raineteau O, Kartje GL, Schwab ME, 1998. Neurite growth inhibitors restrict plasticity and functional recovery following corticospinal tract lesions. Nat. Neurosci 1, 124–131. 10.1038/373 [PubMed: 10195127]

Tong J, Liu W, Wang X, Han X, Hyrien O, Samadani U, Smith DH, Huang JH, 2013. Inhibition of Nogo-66 receptor 1 enhances recovery of cognitive function after traumatic brain injury in mice. J. Neurotrauma 30, 247–258. 10.1089/neu.2012.2493 [PubMed: 22967270]

Tsai SY, Papadopoulos CM, Schwab ME, Kartje GL, 2011. Delayed anti-Nogo-A therapy improves function after chronic stroke in adult rats. Stroke 42, 186–190. 10.1161/STROKEAHA.110.590083 [PubMed: 21088244]

Tucker LB, Burke JF, Fu AH, McCabe JT, 2017. Neuropsychiatric Symptom Modeling in Male and Female C57BL/6J Mice after Experimental Traumatic Brain Injury. J. Neurotrauma 34, 890–905. 10.1089/neu.2016.4508 [PubMed: 27149139]

Vajda F, Jordi N, Dalkara D, Joly S, Christ F, Tews B, Schwab ME, Pernet V, 2015. Cell type-specific Nogo-A gene ablation promotes axonal regeneration in the injured adult optic nerve. Cell Death Differ. 22, 323–335. 10.1038/cdd.2014.147 [PubMed: 25257170]

Villa A, Gelosa P, Castiglioni L, Cimino M, Rizzi N, Pepe G, Lolli F, Marcello E, Sironi L, Vegeto E, Maggi A, 2018. Sex-Specific Features of Microglia from Adult Mice. Cell Rep. 23, 3501–3511. 10.1016/j.celrep.2018.05.048 [PubMed: 29924994]

Vogel A, Wilken-Schmitz A, Hummel R, Lang M, Gurke R, Schreiber Y, Schäfer MKE, Tegeder I, 2020. Low brain endocannabinoids associated with persistent non-goal directed nighttime hyperactivity after traumatic brain injury in mice. Sci. Rep 10, 1–22. 10.1038/s41598-020-71879-x [PubMed: 31913322]

Vorhees CV, Williams MT, 2006. Morris water maze: Procedures for assessing spatial and related forms of learning and memory. Nat. Protoc 1, 848–858. 10.1038/nprot.2006.116 [PubMed: 17406317]

Wang W, Wang J, Tang Q, Zhu X, Zhu R, Cui D, Wei C, Liu Xinjie, Liu Xingxing, Ran S, Pan Y, Yu J, 2021. CX3CR1 deficiency aggravates brain white matter injury and affects expression

of the CD36/15LO/NR4A1 signal. Biochem. Biophys. Res. Commun 549, 47–53. 10.1016/j.bbrc.2021.02.053 [PubMed: 33662668]

Wikström K, Kavanagh DJ, Reid HM, Kinsella BT, 2008. Differential regulation of RhoA-mediated signaling by the TPα and TPβ isoforms of the human thromboxane A2 receptor: Independent modulation of TPα signaling by prostacyclin and nitric oxide. Cell. Signal 20, 1497–1512. 10.1016/j.cellsig.2008.04.006 [PubMed: 18502100]

Willi R, Aloy EM, Yee BK, Feldon J, Schwab ME, 2009. Behavioral characterization of mice lacking the neurite outgrowth inhibitor Nogo-A. Genes, Brain Behav. 8, 181–192. 10.1111/j.1601-183X.2008.00460.x [PubMed: 19077178]

Willi R, Weinmann O, Winter C, Klein J, Sohr R, Schnell L, Yee BK, Feldon J, Schwab ME, 2010. Constitutive genetic deletion of the growth regulator nogo-A induces schizophrenia-related endophenotypes. J. Neurosci 30, 556–567. 10.1523/JNEUROSCI.4393-09.2010 [PubMed: 20071518]

Xiang SY, Dusaban SS, Brown JH, 2013. Lysophospholipid receptor activation of RhoA and lipid signaling pathways. Biochim. Biophys. Acta - Mol. Cell Biol. Lipids 10.1016/j.bbalip.2012.09.004

Yan J, Zhou XFXX-F, Guo J-JJ, Mao L, Wang Y-JJ, Sun J, Sun L-XX, Zhang L-YY, Zhou XFXX-F, Liao H, 2012. Nogo-66 inhibits adhesion and migration of microglia via GTPase Rho pathway in vitro. J. Neurochem 120, 721–731. 10.1111/j.1471-4159.2011.07619.x [PubMed: 22145612]

Yang Y, Liu Y, Wei P, Peng H, Winger R, Hussain RZ, Ben LH, Cravens PD, Gocke AR, Puttaparthi K, Racke MK, McTigue DM, Lovett-Racke AE, 2010. Silencing Nogo-A promotes functional recovery in demyelinating disease. Ann. Neurol 67, 498–507. 10.1002/ana.21935 [PubMed: 20437585]

Yona S, Kim KW, Wolf Y, Mildner A, Varol D, Breker M, Strauss-Ayali D, Viukov S, Guilliams M, Misharin A, Hume DA, Perlman H, Malissen B, Zelzer E, Jung S, 2013. Fate Mapping Reveals Origins and Dynamics of Monocytes and Tissue Macrophages under Homeostasis. Immunity 38, 79–91. 10.1016/j.immuni.2012.12.001 [PubMed: 23273845]

Yu J, Fernández-Hernando C, Suarez Y, Schleicher M, Hao Z, Wright PL, DiLorenzo A, Kyriakides TR, Sessa WC, 2009. Reticulon 4B (Nogo-B) is necessary for macrophage infiltration and tissue repair. Proc. Natl. Acad. Sci. U. S. A 106, 17511–17516. 10.1073/pnas.0907359106 [PubMed: 19805174]

Zemmar A, Chen C-C, Weinmann O, Kast B, Vajda F, Bozeman J, Isaad N, Zuo Y, Schwab ME, 2017. Oligodendrocyte- and Neuron-Specific Nogo-A Restrict Dendritic Branching and Spine Density in the Adult Mouse Motor Cortex. Cereb. Cortex 28, 1–9. 10.1093/cercor/bhx116

Zemmar A, Weinmann O, Kellner Y, Yu X, Vicente R, Gullo M, Kasper H, Lussi K, Ristic Z, Luft AR, Rioult-Pedotti M, Zuo Y, Zagrebelsky M, Schwab ME, 2014. Neutralization of Nogo-A Enhances Synaptic Plasticity in the Rodent Motor Cortex and Improves Motor Learning in Vivo. J. Neurosci 34, 8685–8698. 10.1523/JNEUROSCI.3817-13.2014 [PubMed: 24966370]

Zhang N, Cui Y, Li Y, Mi Y, 2022. A Novel Role of Nogo Proteins: Regulating Macrophages in Inflammatory Disease. Cell. Mol. Neurobiol 10.1007/s10571-021-01124-0

Zheng B, Atwal J, Ho C, Case L, He XL, Garcia KC, Steward O, Tessier-Lavigne M, 2005. Genetic deletion of the Nogo receptor does not reduce neurite inhibition in vitro or promote corticospinal tract regeneration in vivo. Proc. Natl. Acad. Sci. U. S. A 102, 1205–1210. 10.1073/pnas.0409026102 [PubMed: 15647357]

Zheng B, Ho C, Li S, Keirstead H, Steward O, Tessier-Lavigne M, 2003. Lack of enhanced spinal regeneration in Nogo-deficient mice. Neuron 38, 213–224. 10.1016/S0896-6273(03)00225-3 [PubMed: 12718856]

Zheng B, Tuszynski MH, 2023. Regulation of axonal regeneration after mammalian spinal cord injury. Nat. Rev. Mol. Cell Biol 10.1038/s41580-022-00562-y

Zhong J, Fan S, Yan Z, Xiao S, Wan L, Chen C, Zhong S, Liu L, Liu J, 2015. Effects of Nogo-A silencing on TNF- α and IL-6 secretion and TH downregulation in lipopolysaccharide-stimulated PC12 cells. Biomed Res. Int 2015, 817914. 10.1155/2015/817914 [PubMed: 26583134]

Zhu Y, Tong Q, Ye J, Ning Y, Xiong Y, Yang M, Xiao H, Lu J, Xu W, Li J, Li Q, 2017. Nogo-B Facilitates LPS-Mediated Immune Responses by Up-Regulation of TLR4-signaling in Macrophage RAW264.7. Cell. Physiol. Biochem 41, 265–273. 10.1159/000456094 [PubMed: 28214882]

Ziebell JM, Ray-Jones H, Lifshitz J, 2017. Nogo presence is inversely associated with shifts in cortical microglial morphology following experimental diffuse brain injury. Neuroscience 359, 209–223. 10.1016/j.neuroscience.2017.07.027 [PubMed: 28736137]

Zörner B, Schwab ME, 2010. Anti-Nogo on the go: From animal models to a clinical trial. Ann. N. Y. Acad. Sci 10.1111/j.1749-6632.2010.05566.x

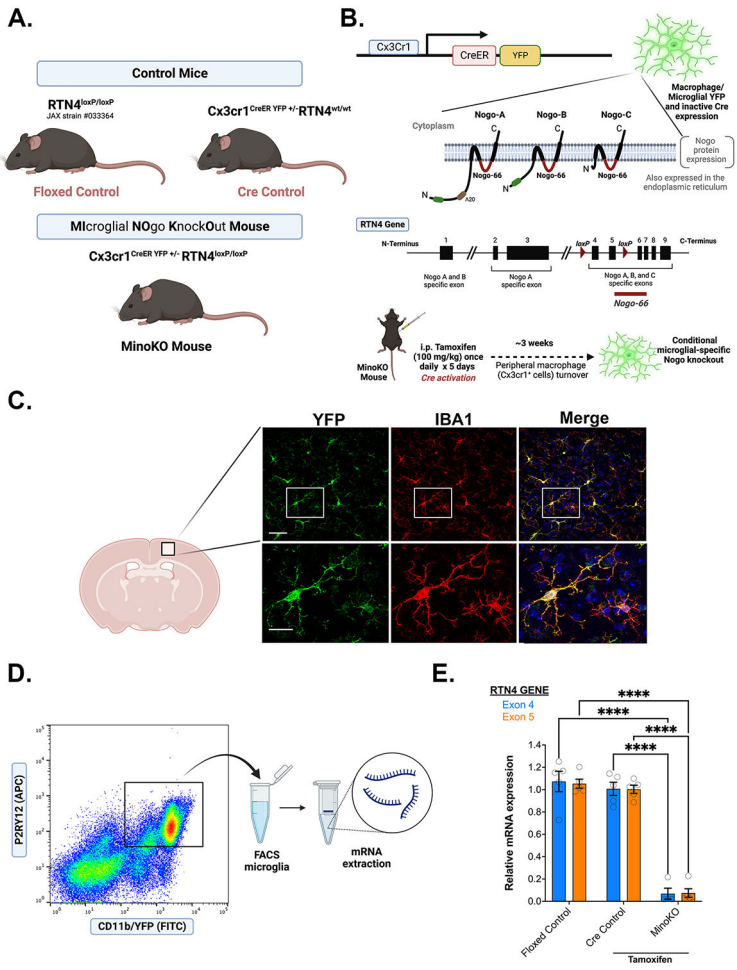

FIGURE 1.

Developing the MinoKO mouse. (a) Mice of three different genotypes were used in the current studies, two different control mice and the inducible microglial Nogo knockout mouse (MinoKO). (b) Both the Cre Control and MinoKO mice express YFP and inactive Cre in Cx3cr1+ cells, which includes peripheral macrophages. The three Nogo proteins, Nogo-A, B, and C, are translated from the RTN4 gene and were targeted with loxP sites placed in a shared region of the gene flanking Exon4 and Exon5. Tamoxifen (TAM) injections activated + cells. Following TAM treatment, peripheral Cx3Cr1+ cells were allowed time to turnover, leaving only the microglia as the recombined cells. (c) YFP expression is highly specific to Iba1+ cells of the brain, indicating expression of Cre is specific to microglia. (d) RNA was isolated from FACS sorted brain cells positive for CD11b and P2Ry12 in both controls and MinoKO mice and analyzed for RTN4 Exon4 and Exon5 gene expression ($n = 4$ animals/group). ANOVA with Tukey's multiple comparison was used for statistical analysis with error bars representing mean ±SEM; $F_{2,23} = 186.4$ **** = $p < 0.0001$.

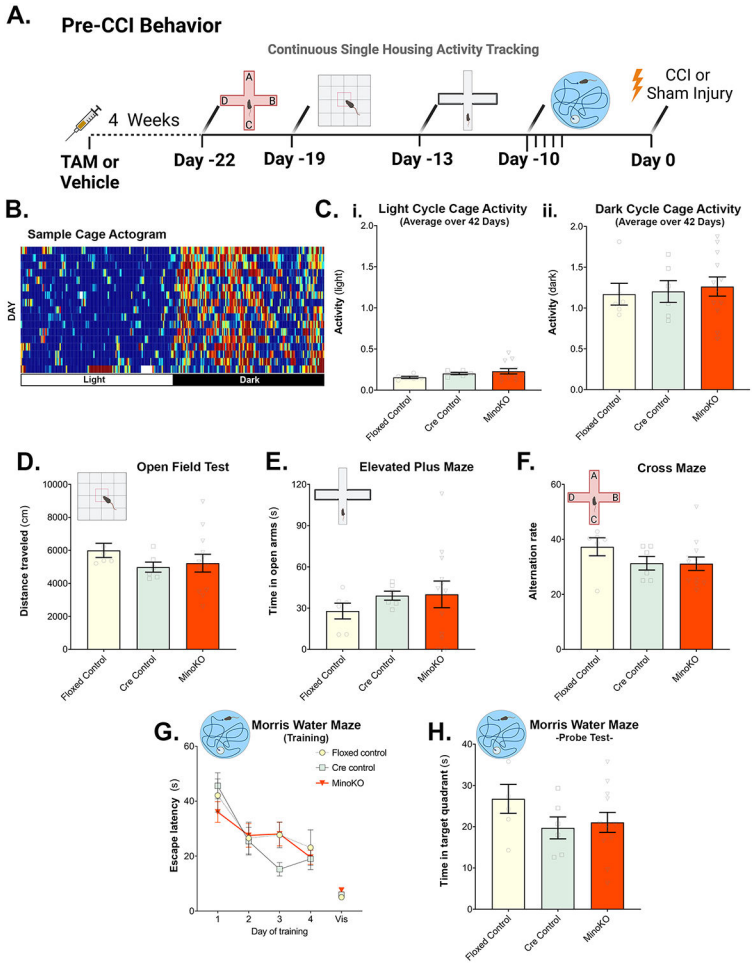

FIGURE 2.

Microglia Nogo-KO has no effect on behavior in healthy mice. (a) Pre-CCI behavioral timeline. (b) Sample actogram showing 17 consecutive days of home cage activity from a singly housed control mouse. Each row is a 24 h period; each vertical bar represents average activity in a 5-min bin. Burst of activity in light cycle on last day represents cage bedding change. (c) Light cycle (i) and dark cycle (ii) activity averages over 42 days. (d) Distance traveled in a 30 min open field test. (e) Time spent with mouse's whole body in either open arm of an elevated plus maze. (f) Alternation rate in a cross maze apparatus. (g) Latency to locate hidden platform, each point representing average of four trials during four consecutive days of training. “Vis” indicates visible platform control trials, which were performed after probe trial. (h) Time spent in target quadrant during 60 s probe test conducted 24 h after last training trial. All behavioral data was not significant between groups assessed via mixed linear model with ANOVA.

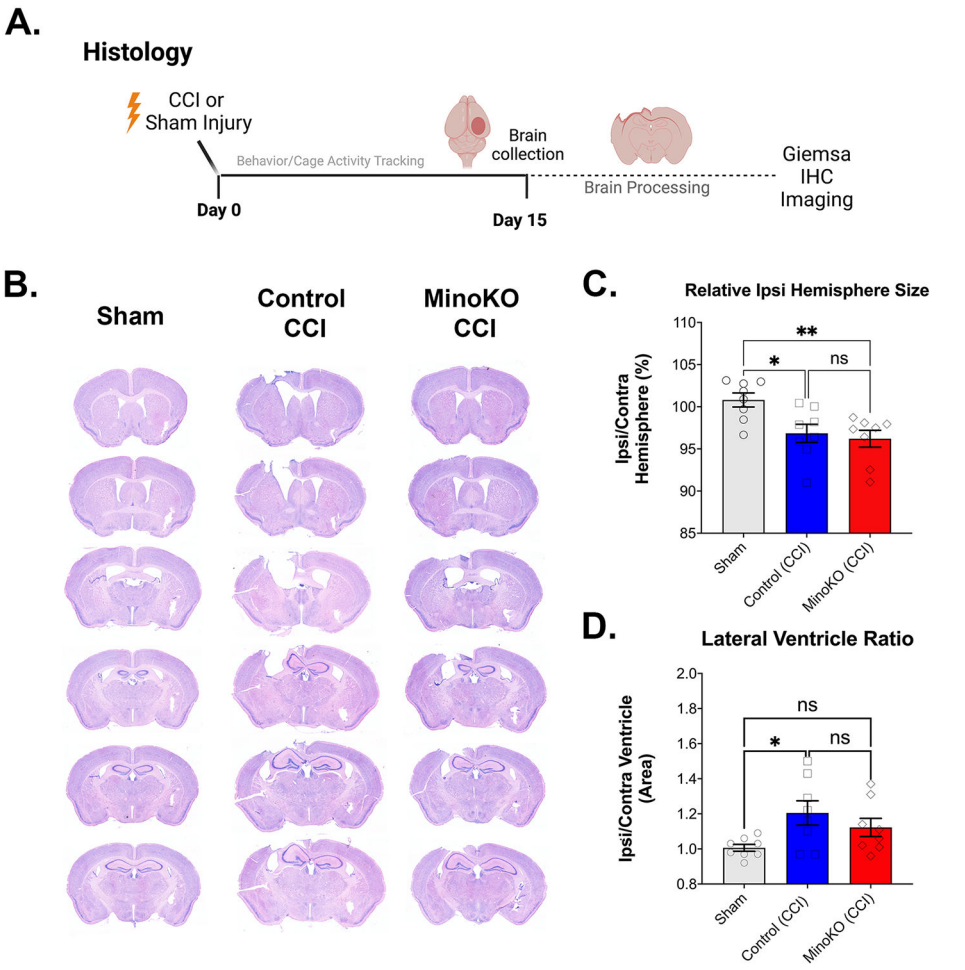

FIGURE 3.

Evaluation of ipsilateral injury size and ventricle volume. Histological assessment timeline for all animals (a). Representative Giemsa stained brain slices from Sham and CCI treated animals. Sham group includes animals from all genotypes; Control-CCI animals include Floxed and Cre Control-CCI treated animals (b). Differences in size of ipsilateral versus contralateral hemisphere represented as a percentage (c). CCI significantly induced loss of tissue in both control and MinoKO mice (c). CCI significantly induced increased lateral ventricle size in the ipsilateral hemisphere of control but not MinoKO-CCI injured mice (d). One-way ANOVA with Tukey's multiple comparison was used for statistical analysis with error bars representing mean ±SEM; ns = not significant, * = $p < 0.05$, and ** = $p < 0.01$.

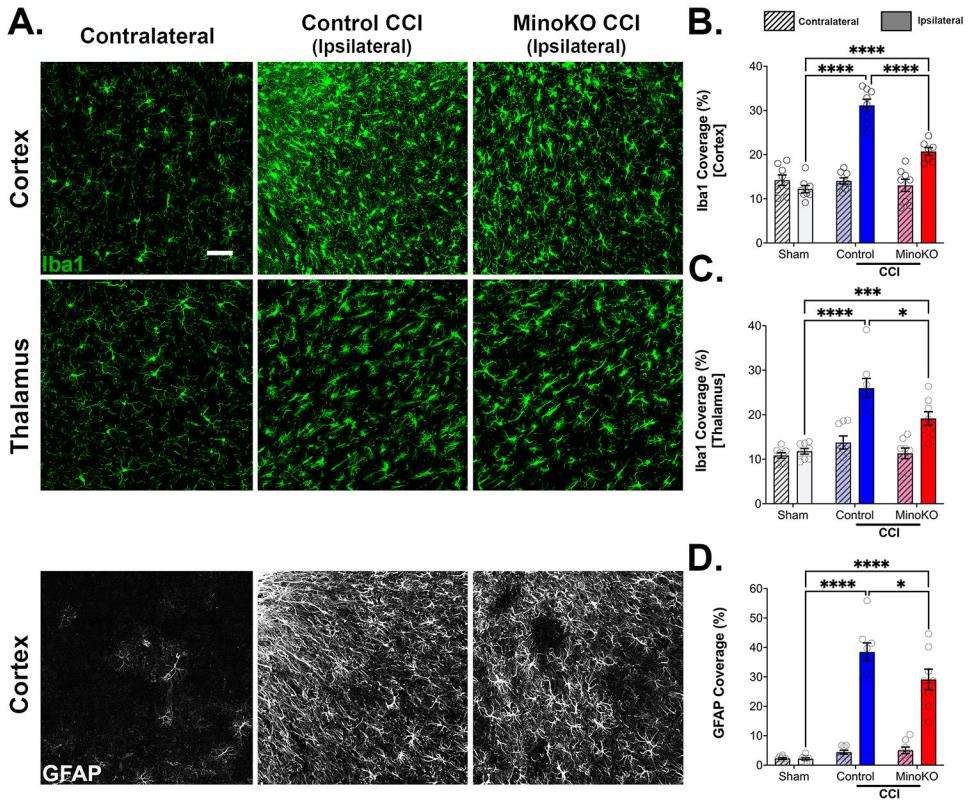

FIGURE 4.

Iba1 (microglia) and GFAP (astrocyte) immunoreactivity 2 weeks post-CCI. Representative immunohistochemistry images in the cortex and thalamus for Iba1 staining and the cortex for GFAP staining. Both contralateral and ipsilateral regions of the brain were assessed for each animal (a). Quantified cortex (b) and thalamus (c) coverage percentage of Iba1 (microglia) immunoreactivity in averaged images across all animals. Quantified cortex coverage percentage of GFAP (astrocyte) immunoreactivity in averaged images across all animals (d). No differences in Iba1 or GFAP were observed for the contralateral regions of the brain. Ipsilateral regions were statistically compared via One-way ANOVA with Tukey's multiple comparison with error bars representing mean ±SEM; * = $p < 0.05$, *** = $p < 0.001$, and **** = $p < 0.0001$. Measure bar= 50 μm and applies across all images.

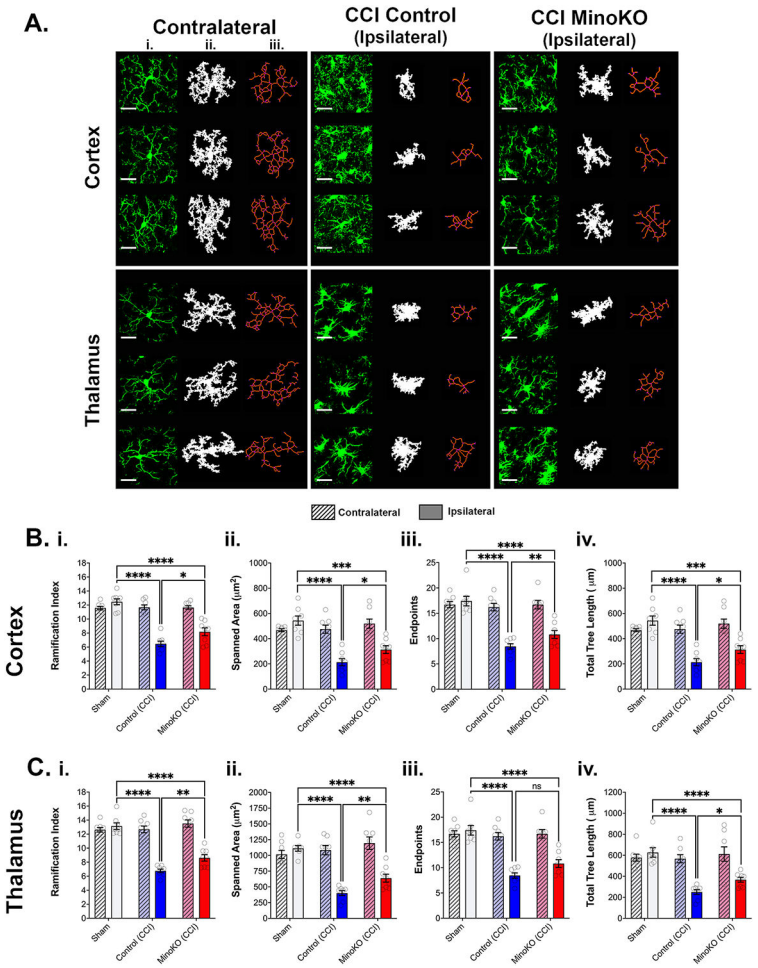

FIGURE 5.

Microglia morphology assessment following TBI in the contra- and ipsilateral hemispheres. Representative maximum intensity projections of Iba1+ microglia (a i) (green) that have been thresholded (a ii) and skeletonized (a iii) for assessment using MotiQ software across treatment group and regions (a). As no differences were observed in contralateral microglia, as determined via one-way ANOVA, for any parameters assessed (b and c), the contralateral group images are representative across all genotypes. Microglia were assessed in both the cortex (b) and thalamus (c) for ramification index (i), spanned area (ii), endpoints (iii), and total tree length (iv). One data point represents the animal mean (20 microglia per region for each animal). Ipsilateral microglia were statistically analyzed via one-way ANOVA with Tukey's multiple comparison with error bars representing mean ±SEM; ns = not significant, * = $p < 0.05$, ** = $p < 0.01$, *** = $p < 0.001$, and **** = $p < 0.0001$. Measure bar = 20 μm.

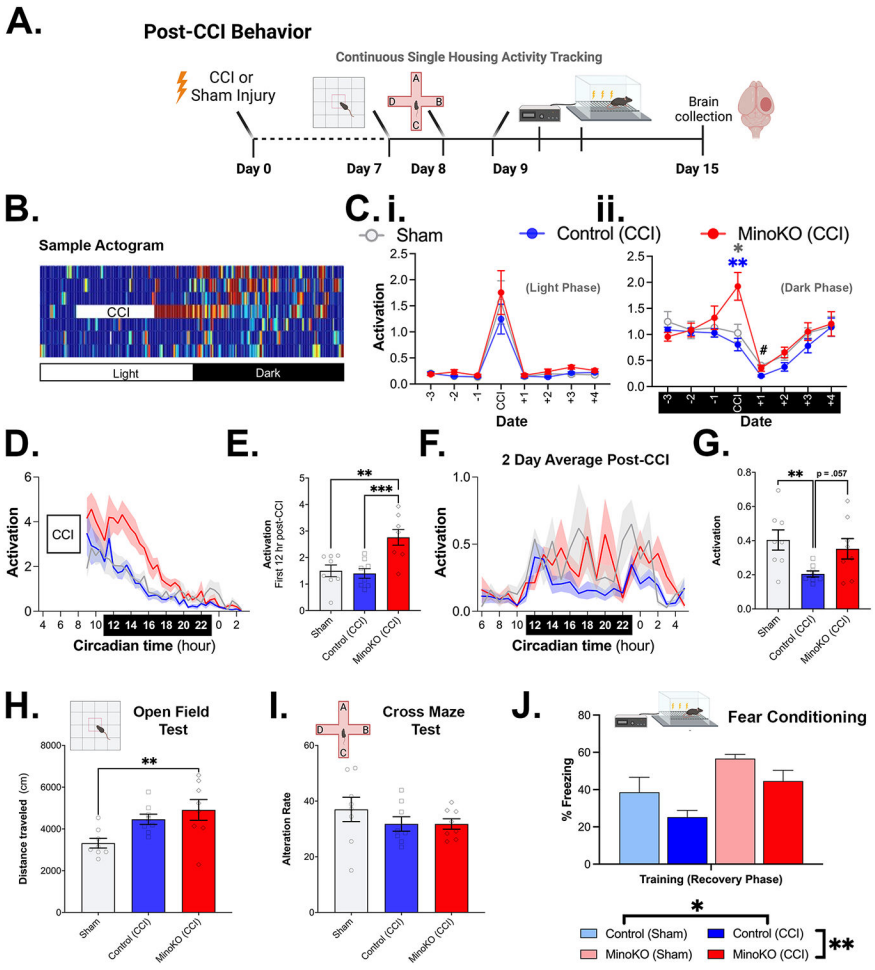

FIGURE 6.

Post CCI behavioral assessment. (a) Timeline for behavior performed following CCI or sham injury. (b) Sample Actogram showing continuous cage tracking data of representative CCI-treated control mouse. Each row represents 24 h; each bar is average activation in a 5-min period. Animals were removed from their cages during the CCI surgery. Day to day average activation (c) during light (i) and dark (ii) phases, excluding 30 mins surrounding phase transitions; Mixed effects analysis, ** = $p < 0.01$ MinoKO-CCI versus Control-CCI and * = $p < 0.05$ MinoKO-CCI v. Sham; # $p < 0.05$ Sham versus Control-CCI. "CCI" indicates day of CCI treatment (Day 0). (d) Home cage activation 12 h following CCI, with each data point representing averaged 2 h blocks of cage activation. (e) Total activation in 12 h immediately after CCI. (f) Within day home cage activation averaged over the first two days following CCI. G) Dark phase 2 days (~30 h) post-CCI. (h) Distance traveled in a 30 min open field test. (i) Alteration rate in a cross maze apparatus. (j) Fear conditioning assessment, including training days. Differences in freezing were observed between genotypes ($p = 0.003$) and CCI treatment ($p = 0.04$). Data was analyzed using a mixed linear analysis with age of mice showing no significant effect on results. ANOVA with Tukey's multiple comparison was used for statistical analysis with error bars representing mean ±SEM; * = $p < 0.05$, ** = $p < 0.01$, and *** = $p < 0.001$.

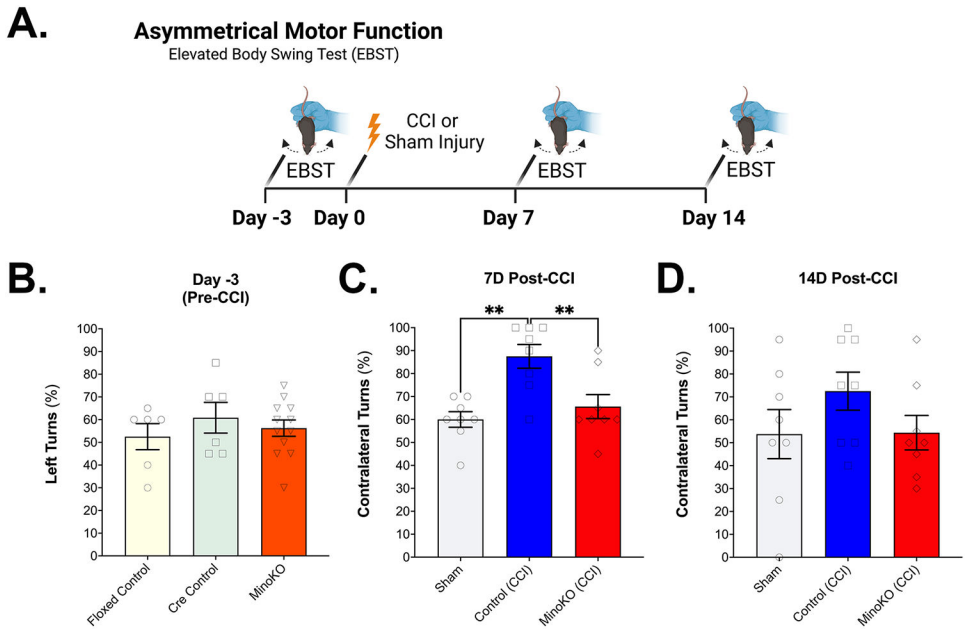

FIGURE 7.

Asymmetrical motor function assessment pre- and post-CCI or sham injury. (a) Timeline of EBST procedures. EBST was performed three days prior to (b) and 7 (c) and 14 days (d) after CCI or sham injury. Animals did not perform differently in the pre-test or two weeks after the CCI injury. One way ANOVA with Tukey's multiple comparison was used for statistical analysis with error bars representing mean ±SEM; ** = $p < 0.01$.

Table 1.

Mice used in experiments. Age at the time of CCI procedure is presented.

Genotype	Sex	Age (mo)	Procedure
Floxed Control	F	4.3	CCI
	M	5	CCI
	M	5	CCI
	M	4.3	CCI
	M	5	SHAM
	F	4.3	SHAM
Cre Control	F	4.2	CCI
	M	5	CCI
	M	5	CCI
	M	5	CCI
	M	5	SHAM
	F	4.2	SHAM
MinoKO	M	5.8	CCI
	M	3.7	CCI
	M	6.3	CCI
	F	5.8	CCI
	F	5.8	CCI
	F	5.8	CCI
	F	4.5	CCI
	F	4.5	CCI
	F	8.6	SHAM
	F	8.6	SHAM
	M	5.9	SHAM
	M	6.3	SHAM

Table 2.

Primer and probe sets used in studies.

Primer/probe set:		
HPRT1:	Forward Primer:	5’- TGA TAG ATC CAT TCC TAT GAC TGT AGA −3’
	Reverse Primer:	5’- AAG ACA TTC TTT CCA GTT AAA GTT GAG −3’
	Probe:	Universal Probe Library: Probe 22 - Roche
RTN4 (Exon 5):	Assay ID:	Mm00445861_m1
	Chromosome Location:	Chr.11: 29692898 - 29744414
	Assay Location	2815
RTN 4 (Exon 4):	Assay ID:	Mm00806750_m1
	Chromosome Location:	Chr.11: 29692898 - 29744414
	Assay Location	2613